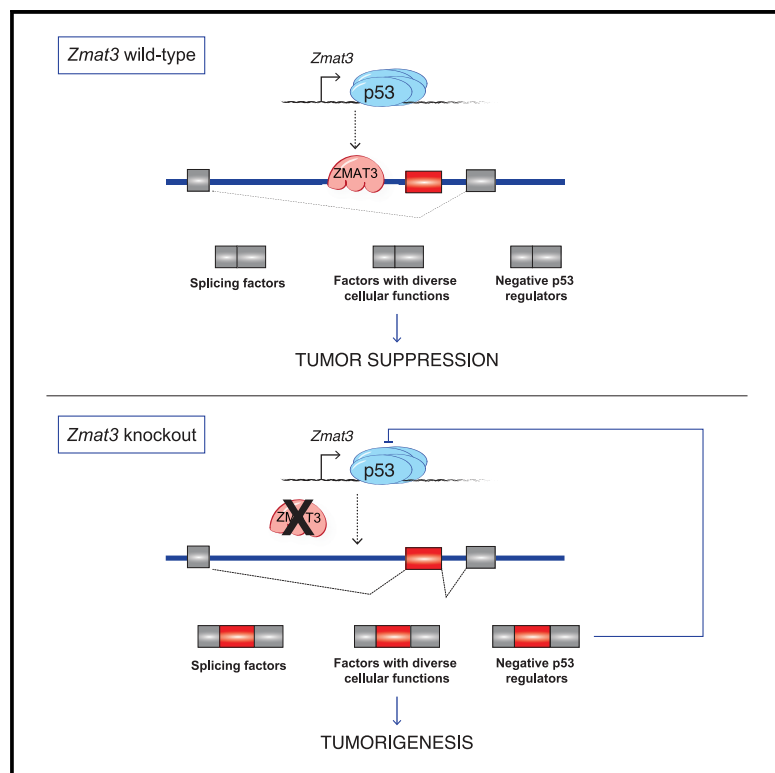


Zmat3 Is a Key Splicing Regulator in the p53 Tumor Suppression Program

Graphical Abstract



Authors

Kathryn T. Bieging-Rolett,
Alyssa M. Kaiser, David W. Morgens, ...,
Monte M. Winslow, Michael C. Bassik,
Laura D. Attardi

Correspondence

attardi@stanford.edu

In Brief

p53 is a critically important but incompletely understood tumor suppressor. Bieging-Rolett et al. identify the p53 target gene *Zmat3*, encoding an RNA-binding protein, as a key tumor suppressor downstream of p53 in a broad range of cancers and uncover a role for *ZMAT3* in regulating alternative RNA splicing.

Highlights

- RNAi and CRISPR screens *in vivo* reveal p53 targets with tumor suppressor activity
- Zmat3 is a tumor suppressor in mouse lung and liver cancers and human carcinomas
- Zmat3 binds RNA with unique positional specificity to regulate RNA splicing
- Zmat3 RNA splicing affects transcripts involved in a variety of cellular processes



Article

Zmat3 Is a Key Splicing Regulator in the p53 Tumor Suppression Program

Kathryn T. Biegling-Rolett,¹ Alyssa M. Kaiser,^{1,8} David W. Morgens,^{2,8} Anthony M. Boutelle,^{1,8} Jose A. Seoane,^{3,4} Eric L. Van Nostrand,⁵ Changyu Zhu,⁶ Shauna L. Houlihan,⁶ Stephano S. Mello,¹ Brian A. Yee,⁵ Jacob McClendon,¹ Sarah E. Pierce,² Ian P. Winters,² Mengxiong Wang,¹ Andrew J. Connolly,⁷ Scott W. Lowe,⁶ Christina Curtis,^{3,4} Gene W. Yeo,⁵ Monte M. Winslow,^{2,4} Michael C. Bassik,^{2,4} and Laura D. Attardi^{1,2,4,9,*}

¹Division of Radiation and Cancer Biology, Department of Radiation Oncology, Stanford University School of Medicine, Stanford, CA 94305, USA

²Department of Genetics, Stanford University School of Medicine, Stanford, CA 94305, USA

³Department of Medicine, Stanford University School of Medicine, Stanford, CA 94305, USA

⁴Stanford Cancer Institute, Stanford University School of Medicine, Stanford, CA 94305, USA

⁵Department of Cellular and Molecular Medicine & Institute for Genomic Medicine, University of California San Diego, La Jolla, CA 92037, USA

⁶Cancer Biology and Genetics Program, Sloan Kettering Institute, Memorial Sloan Kettering Cancer Center, New York, NY 10065, USA

⁷Department of Pathology, UCSF School of Medicine, San Francisco, CA 94143, USA

⁸These authors contributed equally

⁹Lead Contact

*Correspondence: attardi@stanford.edu

<https://doi.org/10.1016/j.molcel.2020.10.022>

SUMMARY

Although *TP53* is the most commonly mutated gene in human cancers, the p53-dependent transcriptional programs mediating tumor suppression remain incompletely understood. Here, to uncover critical components downstream of p53 in tumor suppression, we perform unbiased RNAi and CRISPR-Cas9-based genetic screens *in vivo*. These screens converge upon the p53-inducible gene *Zmat3*, encoding an RNA-binding protein, and we demonstrate that *ZMAT3* is an important tumor suppressor downstream of p53 in mouse *Kras^{G12D}*-driven lung and liver cancers and human carcinomas. Integrative analysis of the *ZMAT3* RNA-binding landscape and transcriptomic profiling reveals that *ZMAT3* directly modulates exon inclusion in transcripts encoding proteins of diverse functions, including the p53 inhibitors MDM4 and MDM2, splicing regulators, and components of varied cellular processes. Interestingly, these exons are enriched in NMD signals, and, accordingly, *ZMAT3* broadly affects target transcript stability. Collectively, these studies reveal *ZMAT3* as a novel RNA-splicing and homeostasis regulator and a key component of p53-mediated tumor suppression.

INTRODUCTION

TP53 is the most commonly mutated gene in human cancers, underscoring its critical role in tumor suppression (Kandoth et al., 2013). p53 is a transcriptional activator that responds to diverse stress signals by regulating gene expression programs that limit neoplastic behavior (Biegling et al., 2014; Vousden and Prives, 2009). The best characterized p53 programs are in response to acute DNA damage, when p53 transcriptionally induces the *p21* CDK inhibitor to trigger cell-cycle arrest and DNA repair or pro-apoptotic BCL2 family members *Puma* and *Noxa* to eradicate damaged cells through apoptosis. The ability of p53 to transactivate target genes is essential for tumor suppression, as *TP53* mutations in humans compromise sequence-specific DNA binding and p53 target gene induction. Moreover, knockin mice expressing a transcriptionally dead p53 mutant with mutations in both transactivation domains

(TADs) phenocopy *p53* null mice in tumor predisposition (Brady et al., 2011; Jiang et al., 2011; Mello et al., 2017).

A variety of mutant mouse strains have been generated to illuminate the gene expression programs downstream of p53 that are most critical to tumor suppression. Analysis of a p53 TAD1 (*p53^{25,26}*) mutant knockin mouse strain revealed that *p53^{25,26}* is severely compromised in activating most p53 target genes—including many classical p53 target genes like *p21*, *Puma*, and *Noxa*—yet retains the ability to activate a small subset of primarily novel target genes (Brady et al., 2011). Interestingly, this mutant is fully competent for suppressing various cancers, including B and T cell lymphomas, medulloblastoma, and lung adenocarcinoma (Brady et al., 2011; Jiang et al., 2011). These findings suggested that noncanonical p53 target genes may be critical for p53-mediated tumor suppression. Further support for this idea came from the analysis of mice expressing *p53^{3KR}*—an acetylation site mutant that cannot activate classical



p53 target genes—and *p21*–/–; *Puma*–/–; *Noxa*–/– mice, neither of which are prone to spontaneous cancers (Li et al., 2012b; Valente et al., 2013). Collectively, these studies suggested that p53-mediated tumor suppression does not require classical p53 target genes, including *p21*, *Noxa*, and *Puma*, or that other genes can compensate for loss of these genes. These studies have thus prompted a renewed investigation of the transcriptional programs underlying p53-mediated tumor suppression (Bieging et al., 2014; Mello and Attardi, 2018).

Recent studies have implicated specific p53-inducible genes in p53-mediated tumor suppression in different settings. In *Myc*-induced hepatocellular carcinoma, p53 induction of *Abca1* and suppression of the mevalonate pathway are important for tumor suppression (Moon et al., 2019). The p53-regulated DNA repair gene *Mlh1* contributes to the suppression of leukemia in an *Eμ-Myc*; *Puma*–/– background (Janic et al., 2018). In pancreatic cancer, a p53-PTPN14-YAP axis operates to suppress the development of this disease (Mello et al., 2017). Despite these recent advances, our understanding of p53 function in tumor suppression remains far from complete. It is unclear, for example, whether different p53 pathways are involved in distinct tumor types and in response to different oncogenic drivers or whether there are core p53 pathways critical for suppression of tumorigenesis in multiple contexts. It would therefore be enlightening to use an unbiased approach to identify p53-inducible genes most fundamental to tumor suppression.

Here, we investigate the p53 transcriptional programs critical for tumor suppression, which will be pivotal not only for understanding the molecular underpinnings of p53 function but also for ultimately gaining insights that would allow development of therapies aimed at the critically important but difficult-to-target p53 pathway. We leverage the tumor-suppression-competent p53^{25,26} mutant to delineate p53 tumor-suppression-associated genes (TSAGs) whose expression is tightly linked to tumor suppression, and we interrogate which TSAGs display tumor suppressor activity using both unbiased RNA interference (RNAi) and CRISPR-Cas9 pooled screens *in vivo*. These studies, coupled with autochthonous mouse model and human cancer genome analyses, unveil the RNA-binding protein (RBP) ZMAT3 as a key tumor suppressor downstream of p53. Molecular analyses reveal a novel function for ZMAT3 in RNA homeostasis via modulating alternative splicing, resulting in multifaceted effects on diverse pathways. These findings establish a ZMAT3-regulated splicing program, providing critical new insight into a core mediator of p53-dependent tumor suppression.

RESULTS

Identification of p53 TSAGs

Identifying p53 target genes critical for tumor suppression has been challenging due to the vast number of p53-regulated genes, as illustrated by the observation that >1,000 genes are induced by p53 in oncogene-expressing fibroblasts (Figures 1A and S1A) (Brady et al., 2011). To identify the most relevant p53-regulated genes for tumor suppression, we sought to pinpoint p53 target genes whose expression is tightly linked to tumor suppression. We leveraged the p53^{25,26} mutant, which activates only a subset of p53 target genes yet is fully compe-

tent for tumor suppression in multiple *in vivo* cancer models (Brady et al., 2011; Jiang et al., 2011). By uncovering the p53-dependent genes still induced by this mutant in neoplastic mouse embryonic fibroblasts (MEFs) expressing Hras^{G12V}—a frequently activated protein in human cancer—we generated a list of 87 genes, which we term p53 TSAGs (Figures 1A and 1B). The majority of p53 TSAGs have one or more p53-bound response elements (REs) near or within their gene body, suggesting that they are direct p53 targets (Table S1; see STAR Methods). Moreover, many p53 TSAGs are p53 inducible in different tumor cell types, including *Eμ-Myc*-driven lymphoma and *Kras*^{G12D}-induced lung adenocarcinoma (LUAD) cells (Figures S1B and S1C). The robust expression of these genes during tumor suppression, coupled with their p53-inducibility in various contexts, supports their potential importance in the p53 tumor suppression program.

RNAi Screening for Functional Tumor Suppressors

To interrogate which of the 87 TSAGs are functionally important for tumor suppression, we first used an *in vivo* pooled short hairpin RNA (shRNA) genetic screening approach. We leveraged an *in vivo* tumor model based on subcutaneous growth of primary MEFs expressing both *E1A* and *Hras*^{G12V} oncogenes (Jiang et al., 2011; Lowe et al., 1994). These cells provide a tractable model with an intact p19ARF-p53 tumor suppressor signaling pathway because they are derived from primary cells and cultured minimally. Importantly, p53 is critical for tumor suppression in this model (Lowe et al., 1994) (Figures S1D–S1F). We generated a lentiviral ultracomplex pooled shRNA library comprising 25 unique shRNAs targeting each TSAG, along with 1,000 negative control (NC) shRNAs (Bassik et al., 2009), a strategy that mitigates the effects of false negative and false positives to ensure sensitivity and efficacy (Figure 1C). After transduction, we subcutaneously injected *E1A;Hras*^{G12V} MEFs into recipient mice and allowed 3 weeks for tumor formation. To identify genes with tumor suppressor function, we determined which shRNAs were enriched relative to the NC shRNAs in the tumors (Figure 1D; Table S2; see STAR Methods). The gene represented by the highest number of enriched shRNAs (10) was *Zmat3*, followed by *Ptpn14*, *Trp53inp1*, and *Dennd2c*, with at least 7 shRNAs detected per gene (Figure 1D; Table S2). We validated these hits by expressing individual enriched shRNAs in *E1A;Hras*^{G12V} MEFs, which increased anchorage-independent growth relative to control cells (Figures 1E, S1G, and S1H), demonstrating that these genes suppress transformation. Interestingly, we recently independently identified *Ptpn14* as a novel p53 target gene with tumor suppressor activity in pancreatic cancer (Mello et al., 2017), and *Trp53inp1* has tumor suppressor activity in mouse models (Al Saati et al., 2013; Cano et al., 2009). Notably, the top hits encode proteins with diverse cellular functions: ZMAT3 encodes a zinc finger RBP (Israeli et al., 1997; Varmeh-Ziae et al., 1997), PTPN14 is a protein tyrosine phosphatase that negatively regulates the YAP oncprotein (Mello et al., 2017), TRP53INP1 is a negative regulator of reactive oxygen species (Cano et al., 2009), and DENND2C is a RAB-GEF (Yoshimura et al., 2010), supporting the idea that p53 modulates multiple distinct pathways to suppress cancer. Accordingly, no single gene knockdown had an effect as dramatic as p53

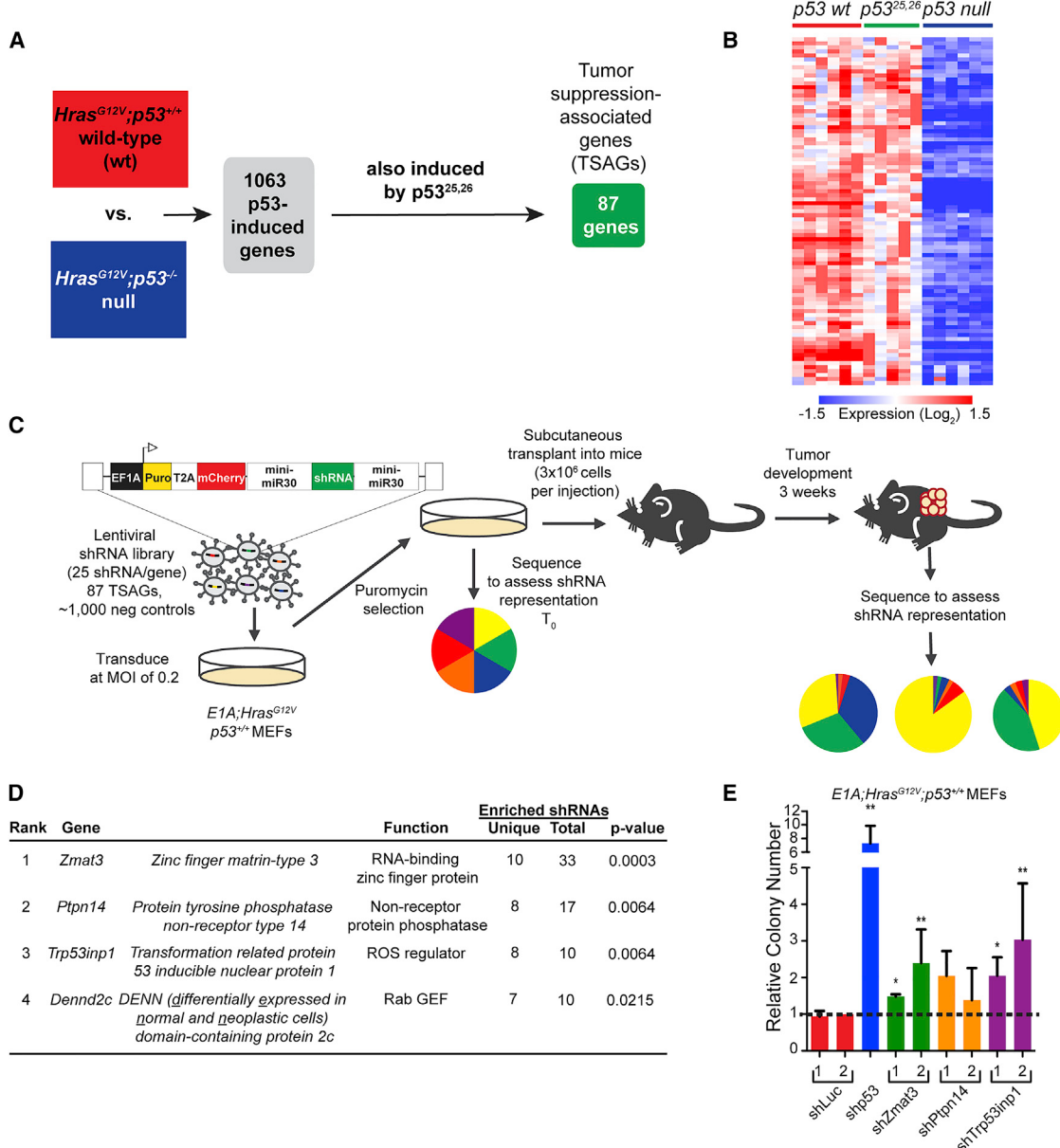


Figure 1. Identification and Functional Screening of p53 Tumor-Suppression-Associated Genes (TSAGs)

(A) Bioinformatics analyses reveal 1,063 genes activated by p53 in *Hras^{G12V}* MEFs, 87 of which are also activated by the p53^{25,26} mutant (TSAGs). (B) Heatmap of expression of 87 p53 TSAGs in *Hras^{G12V}* MEFs homozygous for p53^{WT}, p53^{25,26}, or p53 null alleles. Columns represent independent MEF lines. (C) *E1A;Hras^{G12V};p53^{+/+}* MEFs transduced with a lentiviral shRNA library were collected before transplantation (T₀) and after 3 weeks of subcutaneous growth in *Scid* mice to assess shRNA representation.

(D) Top TSAG hits (n = 9 tumors). “Unique” refers to the number of unique shRNAs enriched relative to negative controls in the nine tumors, “Total” accounts for the same shRNAs enriched in multiple tumors. p values, hypergeometric test.

(E) Soft agar assay. Mean colony number ± SD of three independent *E1A;Hras^{G12V};p53^{+/+}* MEFs lines (each in triplicate) after expression of individual shRNAs. Data are relative to shLuc shRNAs. *p < 0.05 and **p < 0.01, two-tailed paired t test.

knockdown (Figure 1E), consistent with the notion that activation of a network of genes by p53 is critical for tumor suppression (Andrysik et al., 2017; Bieging et al., 2014). Overall, the success of the screen is underscored by both the unbiased identification of known tumor suppressors and the discovery of potential new tumor suppressors, including *Zmat3* and *Dennd2c*.

CRISPR-Cas9 Screening for Functional Tumor Suppressors

While we identified several functional tumor suppressor genes using shRNA screening, we reasoned that a gene deletion screen using CRISPR-Cas9 technology could both reinforce our findings and unveil additional tumor suppressor genes

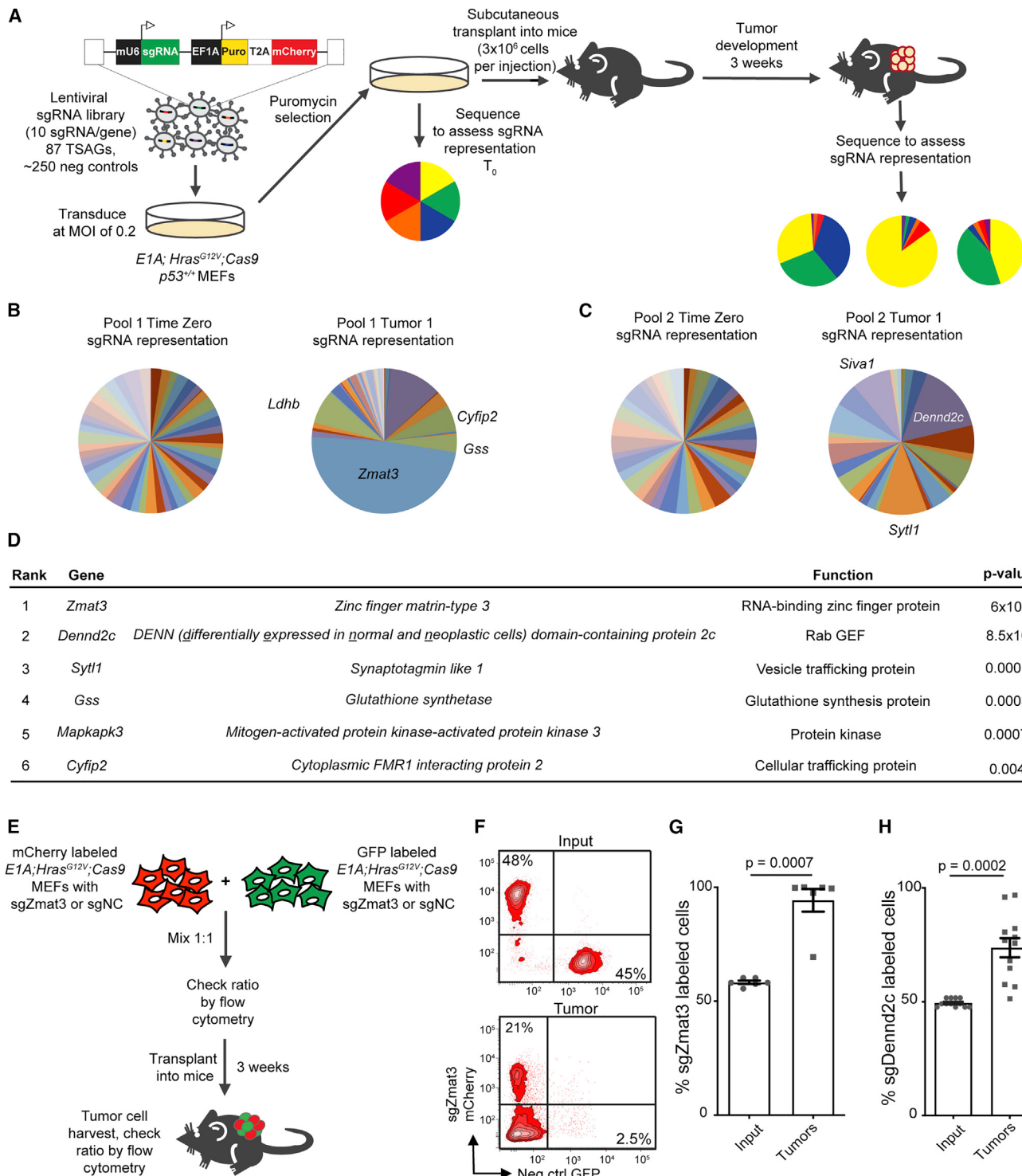


Figure 2. Pooled CRISPR-Cas9 Screen Identifies Functional Tumor Suppressors

(A) E1A;Hras^{G12V};p53^{+/+};Cas9 MEFs transduced with lentiviral sgRNA libraries were collected before transplant at T₀ and after 3 weeks of subcutaneous growth in Scid mice to assess sgRNA representation.

(B and C) Pie charts show representation of sgRNAs (grouped by gene) in each pool (B, pool 1; C, pool 2) at T₀ and in example individual tumors.

(D) Top TSAG hits ranked by enrichment of sgRNAs in tumors relative to T₀ (n = 6 tumors). p values, Mann-Whitney U test.

(E) E1A;Hras^{G12V};p53^{+/+};Cas9 MEFs expressing fluorescent markers and sgZmat3 or negative control sgRNAs were mixed 1:1, injected subcutaneously into Scid mice, and grown for 3 weeks. Dissociated tumor cells were analyzed by FACS.

(legend continued on next page)

(Morgens et al., 2016). We generated lentiviral libraries expressing 10 single guide RNAs (sgRNAs) targeting each of the 87 TSAGs in two pools, with 40–50 TSAGs and 250 NC sgRNAs per pool. Our screening approach was similar to that described above, except that we transduced *E1A;Hras^{G12V}*-expressing MEFs derived from Cas9-transgenic mice (Chiou et al., 2015) with the lentiviral sgRNA libraries. We injected *E1A;Hras^{G12V}*;Cas9 MEFs subcutaneously into recipient mice and allowed 3 weeks for tumor formation (Figure 2A). For each of the two libraries, we quantitatively measured enrichment of individual sgRNA elements in tumors relative to input cells to identify genes with significant tumor suppressor activity in individual tumors (Morgens et al., 2016). Strikingly, in tumors derived from pool 1, sgRNAs targeting *Zmat3* dominated every tumor, bolstering our shRNA screen results (Figures 2B, S2A, and S2C; Table S3). In pool 2, sgRNAs targeting *Dennd2c* were the most significantly enriched, again reinforcing the shRNA screen results (Figures 2C, S2B, and S2D). Interestingly, while sgRNAs targeting other genes showed less enrichment, examination of sgRNA behavior across all tumors identified several additional putative tumor suppressors, such as *Syt1* and *Gss*, which encode a vesicle trafficking protein (Johnson et al., 2012) and glutathione synthetase (Oppenheimer et al., 1979), respectively (Figures 2D, S2C, and S2D; Table S3).

As *Zmat3* and *Dennd2c* were the most significant hits in independent screens using two technologies, we further probed their tumor suppressor capacity. We first performed *in vivo* competition experiments to quantitatively examine the growth advantage of *Zmat3*-deficient cells relative to control cells using *E1A;Hras^{G12V}*;Cas9 MEFs. Individual *Zmat3* or NC sgRNAs were expressed from vectors containing either a GFP or mCherry marker. Next, we mixed NC sgRNA and sgZmat3-expressing cells expressing different fluorophores 1:1, verified the mixed composition by flow cytometry, injected the cells subcutaneously into recipient mice, and analyzed the resulting tumors 3 weeks later by flow cytometry (Figures 2E, 2F, and S2E). *Zmat3*-deficient cells consistently dominated the tumors, underscoring the *in vivo* growth advantage conferred by *Zmat3* deficiency and validating *Zmat3* tumor suppressor activity (Figures 2F and 2G). Similar experiments with *Dennd2c* sgRNAs revealed that *Dennd2c* inactivation also conferred a clear growth advantage *in vivo*, confirming its tumor suppressor capacity (Figures 2H and S2F). Thus, the combined RNAi and CRISPR-Cas9 screening approach converged on two potent tumor suppressors, *Zmat3* and *Dennd2c*.

Zmat3 Expression Is Highly p53 Dependent in Mouse and Human Cells

We next sought to evaluate the role of *Zmat3* and *Dennd2c* as central components of the p53 tumor suppressor network by assessing how universally p53 regulates them. In mouse cells, both *Zmat3* and *Dennd2c* display p53-dependent expression in diverse cell types, including *E1A;Hras^{G12V}* MEFs, *Eμ-Myc* lym-

phoma cells, and embryonic neural crest cells, and *Zmat3* expression is p53 dependent in *Kras^{G12D}*-driven LUAD cells (Figure 3A) (Bowen et al., 2019). Strikingly, in human fibroblasts and in many human cancer types—including breast (BRCA), lung (LUAD), and liver (LIHC) cancers—*ZMAT3* expression is higher in p53-proficient samples than in p53-deficient samples, supporting the notion that *ZMAT3* is broadly a p53 target (Figures 3B and 3C). *DENND2C*, while demonstrating clear p53-dependent expression in human fibroblasts, showed more tissue-specific p53 dependency across cancer types (Figures 3B, 3D, and S3A). These findings suggest that *DENND2C* might play a more tissue-restricted role in p53-mediated tumor suppression.

The marked p53-dependent expression of *ZMAT3* in many human cancer types prompted a deeper investigation of *ZMAT3* regulation by p53. Our chromatin immunoprecipitation sequencing (ChIP-seq) data from both human and mouse cells indicated that the *ZMAT3* locus is directly bound by p53 (Figures 3E and 3F) (Kenzelmann Broz et al., 2013; Younger et al., 2015). Although previous sequence analysis identified several p53 REs in the mouse *Zmat3* promoter (Wilhelm et al., 2002), our ChIP-seq analyses revealed a major p53-bound region containing a perfect p53 RE in the first intron of mouse *Zmat3* and a near-perfect p53 RE in the first intron of human *ZMAT3* (Figures 3E and 3F). To assess the importance of p53 regulation for *Zmat3* expression, we designed sgRNAs to disrupt the p53 RE at the major p53-binding peak in mouse *Zmat3* (Figure 3F). Perturbing this RE in *E1A;Hras^{G12V}*;Cas9 MEFs significantly reduced p53 binding to *Zmat3*, but not to *Cdkn1a*, in ChIP experiments (Figures 3G and S3B) and significantly decreased *Zmat3* mRNA and protein levels similarly to p53 knockout (Figures 3H and 3I), suggesting that the RE is critical for p53 regulation of *Zmat3*. Together, these findings demonstrate that *ZMAT3* is broadly regulated by p53 in numerous mouse and human cell types and that robust *Zmat3* expression relies on direct induction by p53.

Zmat3 Suppresses LUAD and HCC Development

While the oncogene-expressing MEF discovery platform indicated the importance of *Zmat3* in tumor suppression in one context, we sought to interrogate whether *Zmat3* might be more broadly relevant as a tumor suppressor using *in vivo* carcinoma models. p53 plays a key tumor suppressive role in LUAD, with nearly half of human tumors carrying *TP53* mutations (Kandoth et al., 2013). Moreover, both our cell culture data (Figure 3A) and *in vivo* data from mouse tumors (Figure 4A) (Feldser et al., 2010) indicate that *Zmat3* is robustly induced by p53 in LUAD. We thus investigated the role of *ZMAT3* as a tumor suppressor using CRISPR-Cas9-mediated genome editing in an autochthonous *Kras^{G12D}*-driven mouse LUAD model (Jackson et al., 2001; Rogers et al., 2017). We induced tumors in *Kras^{LSL-G12D/+};Rosa26^{Lsl-TdTomato/Lsl-TdTomato};H11^{LSL-Cas9/LSL-Cas9} (KT;H11^{LSL-Cas9}) mice with lentiviruses expressing Cre recombinase and an sgRNA targeting p53, one of three sgRNAs targeting *Zmat3*, or either of two*

(F) Representative FACS plots show input and tumor populations where the negative control sgRNA cells were labeled with GFP and the sgZmat3 cells with mCherry.

(G and H) Plots show the mean percentages ± SEM of cells expressing the sgZmat3 fluorescent label (G) or sgDennd2c fluorescent label (H) relative to all labeled cells (either GFP or mCherry) in both input and tumor populations; n = 6 tumors in (G), n = 12 in (H). p values, two-tailed paired t test.

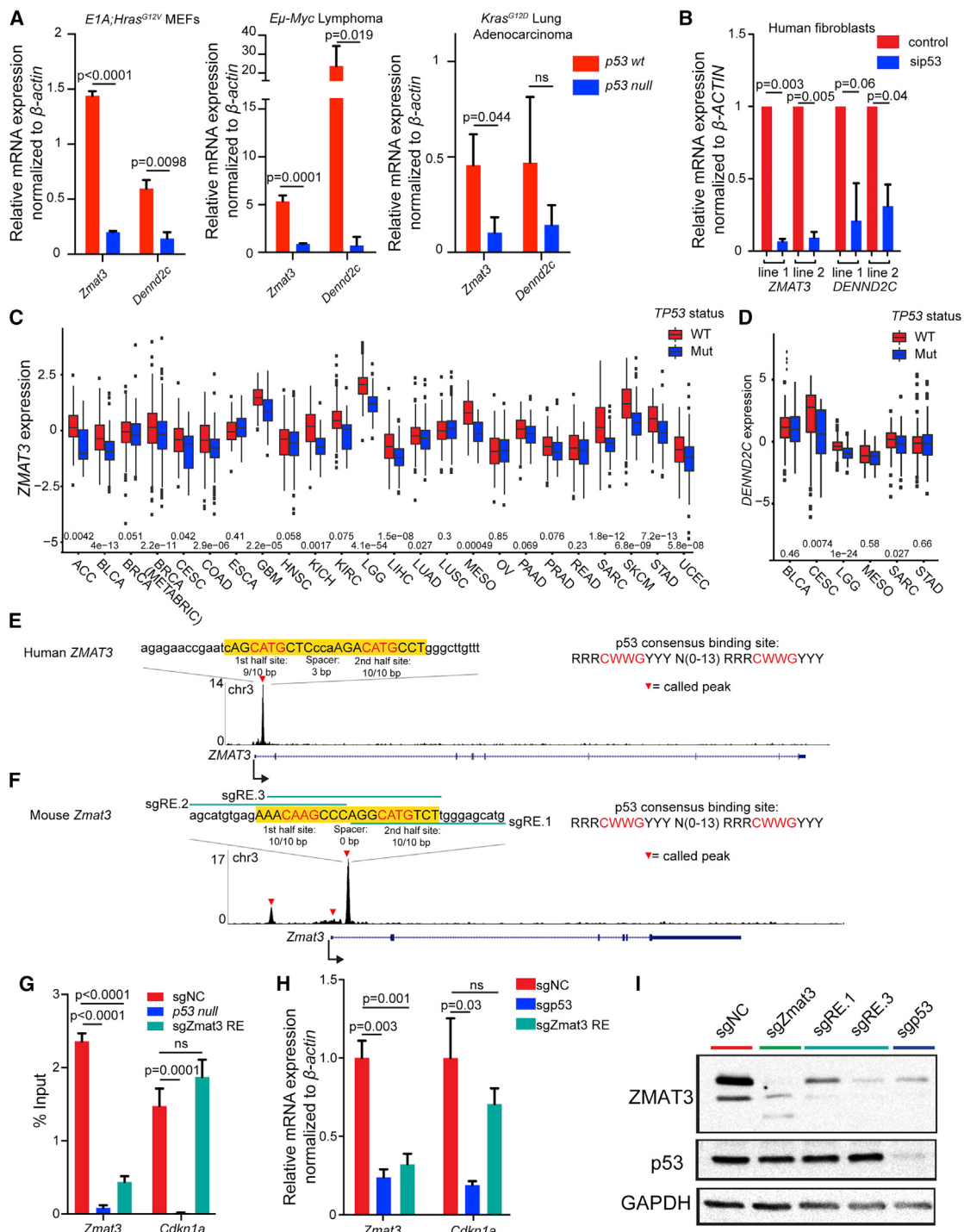


Figure 3. ZMAT3 Expression Is Highly p53 Dependent in Mouse and Human

(A) qRT-PCR analysis of mean expression \pm SD of *Zmat3* and *Dennd2c* in *p53^{WT}* and *p53 null* *E1A;Hras^{G12V}* MEFs, *E μ -Myc* lymphoma cells, and *Kras^{G12D}* LUAD cells, relative to β -actin. p values, two-tailed unpaired t test of different MEF lines ($n = 3$), *Kras^{G12D}* LUAD cell lines ($n = 3$), or technical replicates (*E μ -Myc* lymphoma cell line, $n = 1$). ns, not significant.

(B) qRT-PCR analysis of mean expression \pm SD (technical replicates) of *ZMAT3* and *DENND2C* in primary human fibroblasts transfected with *sip53* or a non-targeting siRNA, relative to β -ACTIN. p values, two-tailed unpaired t test of technical replicates.

(C and D) *ZMAT3* expression (C) or *DENND2C* expression (D) (adjusted for copy number) was mean-centered to zero to allow comparison of samples with wild-type or mutant *TP53* in TCGA datasets. The upper and lower hinges correspond to the first and third quartiles, the upper and lower whiskers show the 1.5 interquartile ranges, and the center line is the median. p values, two-tailed t test.

(legend continued on next page)

NC sgRNAs (Chiou et al., 2015) (Figure 4B). After transduction of lung epithelial cells, Cre excises the Lox-Stop-Lox cassettes, allowing *Kras^{G12D}*, Cas9, and *tdTomato* reporter expression. As anticipated, Cas9-mediated inactivation of p53 led to significantly larger tumors and greater total tumor burden than in NC *KT;H11^{LSL-Cas9}* mice (Figures 4C, 4D, and 4G). Interestingly, Cas9-induced *Zmat3* inactivation also drove significantly larger tumors and greater tumor burden than in control mice (Figures 4E, 4F, 4H, S4A, and S4B). The increase in LUAD growth observed with *Zmat3* inactivation was less than with *p53* inactivation, supporting the idea that *Zmat3* is one critical component of the p53 tumor suppression program. Furthermore, we found that like *p53*, ZMAT3 impeded proliferation without inducing apoptosis, suggesting that proliferation inhibition is a mechanism for suppressing LUAD growth (Figures 4I, 4J, and S4C). We did not observe a similar increase in tumor size when tumors were induced in *p53*-deficient *KPT;H11^{LSL-Cas9}* mice, suggesting that *Zmat3* is most relevant in the context of an intact *p53* pathway (Figure S4D).

To assess the importance of *Zmat3* in suppressing tumorigenesis in an additional autochthonous carcinoma model, we used a mouse hepatocellular carcinoma (HCC) model in which *p53* is tumor suppressive (Tschaharganeh et al., 2014). In this model, a recombinant transposon vector expressing *Kras^{G12D}*, along with vectors expressing Cas9/sgRNAs and Sleeping Beauty transposase, are introduced into hepatocytes via hydrodynamic tail vein injection (HTVI). We used the HTVI model to deliver sgRNAs targeting chromosome 8 (negative control), *p53* (positive control), or *Zmat3* (Figure 4K). Interestingly, while no tumors developed in the sgChrom8 negative control group (0/5), 5/5 mice in both sg*Zmat3* cohorts and the sgp*p53* cohort developed tumors (Figure 4L). Although the penetrance of the tumor phenotype was equivalent in the sgp*p53* group and both sg*Zmat3* groups, the tumors in the sgp*p53* mice were larger than in the sg*Zmat3* mice, again suggesting that *Zmat3* is one component downstream of *p53* (Figures 4M and 4N). Together, these findings illuminate *Zmat3* as a *p53* target gene critical for carcinoma suppression *in vivo*.

ZMAT3 Is a Component of the p53 Pathway in Human Carcinomas

Given the highly conserved regulation of ZMAT3 by *p53* in human cells and the clear tumor suppressor activity of *Zmat3* in mice, we next sought to examine the role of ZMAT3 in the *p53* tumor suppressor pathway in human cancer. We first queried the association between ZMAT3 expression and patient prognosis in human carcinomas. We analyzed a large cohort of breast cancer patients for whom long-term follow-up data (>15 years) are available and with nearly 2,000 tumors for which *TP53* status

is known (Curtis et al., 2012; Pereira et al., 2016). We found that patients with tumors with relatively low ZMAT3 expression exhibited reduced disease-specific survival relative to those with higher ZMAT3 expression. Importantly, this association was only observed for patients with tumors of wild-type *TP53*, but not mutant *TP53*, status (Figures 5A–5C). As predicted from our mouse studies, examination of TCGA LUAD and LIHC data revealed a similar survival pattern for patients with high and low ZMAT3 expression specifically in the context of wild-type *TP53*, although the survival difference in the LUAD data did not reach statistical significance (Figures 5D–5F and S5A–S5C). These correlative findings further support a role for ZMAT3 particularly in cancers in which *p53* is intact.

To further investigate the role for ZMAT3 in the human *p53* tumor suppression program, we leveraged TCGA data to examine patterns of ZMAT3 mutations relative to *TP53* mutations. While amplifications of chromosome 3q where ZMAT3 resides are observed in certain human cancers—potentially due to linkage to the *PIK3CA* oncogene—point mutations in ZMAT3 are also found in some cancers, such as uterine corpus endometrial carcinoma (UCEC) (Cerami et al., 2012; Gao et al., 2013). Interestingly, mutations and deletions in ZMAT3 are mutually exclusive with mutations and deletions in *TP53* in UCEC, supporting the notion that ZMAT3 is a component of *p53*-mediated tumor suppression in humans (Figure 5G).

To examine the functional significance of the *TP53*-ZMAT3 axis in human cancer, we mined data from Project Achilles, a compilation of genome-scale pooled screens from 485 cell lines (Meyers et al., 2017). We specifically interrogated the functional effect of ZMAT3 knockout by CRISPR-Cas9 in human carcinoma cell lines. We parsed the cell lines based on *TP53* status into either wild type or aberrant and plotted the CERES dependency score (Meyers et al., 2017) for each group. Interestingly, we found a significant positive dependency score for ZMAT3 in cell lines with wild-type *p53*, suggesting faster growth of the cell lines with ZMAT3 knockout (Figure 5H). In contrast, cell lines with aberrant *TP53* were unaffected by ZMAT3 perturbation. Furthermore, the top ZMAT3 co-dependencies not only include *TP53* and the *p53* positive regulator *TP53BP1* (with dependency scores positively correlated with that of ZMAT3), but also *p53* negative regulators—*MDM4* and *PPM1D* (with dependency scores negatively correlated with that of ZMAT3; Figure 5I). These functional studies thus further emphasize a growth-suppressive role for ZMAT3 in human cells, particularly when *p53* is intact.

ZMAT3 Is Sufficient to Inhibit Proliferation

Our findings suggesting that ZMAT3 is particularly important for tumor suppression in the context of intact *p53* may be due to a

(E and F) p53 binding profile from human fibroblast (E) and MEF (F) ChIP-seq data shows called peaks (red triangles). The p53 RE is highlighted in yellow, with the nucleotides exactly matching the consensus motif in capital letters and the core motif in red.

(G–I) *E1A;Hras^{G12V};p53^{+/+};Cas9* MEFs were transduced with the p53 RE, *p53*, *Zmat3*, or NC sgRNAs. Any of three sgRNAs were used to disrupt the p53 RE in the largest p53 binding peak (green lines in F).

(G) ChIP assays for p53 binding at the *Zmat3* or *Cdkn1a* locus. Graph shows the mean percent of input recovered ± SEM (n = 6–12 combined technical and biological replicates). p values, two-tailed unpaired t test.

(H) qRT-PCR analysis of mean expression ± SD of *Zmat3* and *Cdkn1a* relative to *β-actin* (n ≥ 3 per line). p values, two-tailed unpaired t test.

(I) ZMAT3 and *p53* protein levels analyzed by western blotting with GAPDH loading control (n ≥ 3).

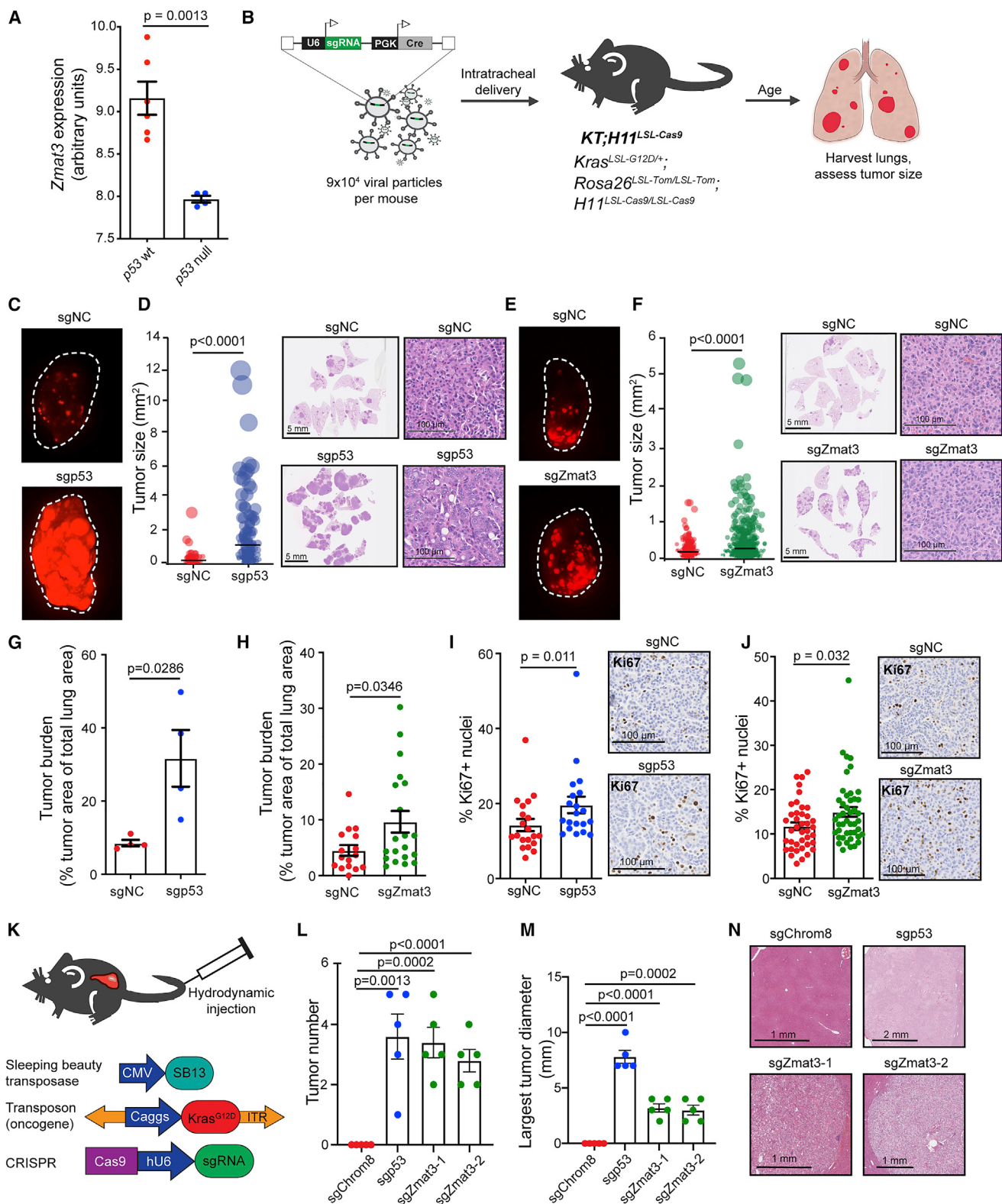


Figure 4. Zmat3 Suppresses Kras^{G12D}-Driven LUAD and HCC

(A) Published microarray analyses of mean \pm SEM of Zmat3 expression in grade 3 *Kras*^{L22D/+}, *Trp53*^{LSL/LSL}; *Rosa26*^{CreERT2} tumors lacking or expressing p53 (Feldser et al., 2010).

(B) Lentiviral vectors expressing Cre recombinase and p53, Zmat3, or NC sgRNAs were used to induce tumors in *KT;H11*^{LSL-Cas9} mice. Lungs were harvested after 17–20 weeks.

(legend continued on next page)

requirement for p53 for efficient *Zmat3* expression (Figure 3I), and therefore, modulating *Zmat3* in a p53-deficient context where *Zmat3* expression is very low might have little effect. Moreover, ZMAT3 might have a more prominent role in the setting of an active p53 pathway based on its cooperation with other p53 target genes. Alternatively, ZMAT3 might act to reinforce p53 function, rendering ZMAT3 ineffective in a p53 null context. To distinguish these possibilities, we asked whether overexpression of ZMAT3 is sufficient to inhibit proliferation in the absence of p53. We overexpressed hemagglutinin (HA)-tagged ZMAT3, p53, or GFP as a negative control in *Kras*^{G12C}-expressing, p53-deficient H23 human LUAD cells and in p53 null untransformed MEFs and assessed proliferation by measuring BrdU incorporation. In both cell types, ZMAT3 overexpression inhibited proliferation, consistent with it acting downstream of p53 (Figures 5J, 5K, and S5D). Importantly, one recurrent ZMAT3 mutation found in human cancers, R99Q, rendered ZMAT3 unable to inhibit proliferation, supporting the notion that ZMAT3 is functionally inactivated by point mutations found in human cancers (Figures 5J and S5D). Notably, the arrest caused by ZMAT3 overexpression is not as potent as that seen with p53 overexpression, suggesting that other factors also contribute to p53-mediated cell-cycle arrest. These data demonstrate not only that ZMAT3 functions downstream of p53, but also that p53 is dispensable for ZMAT3 to inhibit proliferation.

Zmat3 Is an Alternative Splicing Regulator

Given the importance of ZMAT3 as a tumor suppressor, we next explored its mechanism of action. ZMAT3 contains three zinc fingers, the first two of which mediate RNA binding (Israeli et al., 1997; Méndez-Vidal et al., 2002). To identify RNAs directly bound by ZMAT3, we performed enhanced crosslinking and immunoprecipitation (eCLIP) with ZMAT3 antibodies followed by high-throughput sequencing (Van Nostrand et al., 2016). We identified hundreds of ZMAT3-binding peaks (Figures 6A and S6A; Table S4), and analysis of bound RNAs by functional annotation revealed several enriched gene ontology (GO) terms, including RNA binding and mRNA splicing (Figure 6B). To integrate ZMAT3 binding with effects on gene expression, we performed RNA-seq on *E1A;Hras*^{G12V};Cas9 MEFs expressing *Zmat3* or NC sgRNAs (Figure S6B). Comparison of the gene expression profiles of sgNC and sgZmat3-ex-

pressing cells revealed 847 significantly differentially expressed genes (Figure 6C; Table S5). GO term annotation again uncovered various categories related to RNA biology, such as RNA binding, nucleolus, and mRNA splicing, suggesting a fundamental role for ZMAT3 in RNA regulation (Figure 6D). Overlapping ZMAT3-bound and regulated transcripts revealed 95 transcripts, again associated with RNA-related processes, including RNA binding and mRNA splicing (Figure 6E). Together, these findings suggest a broad role for ZMAT3 in RNA homeostasis.

eCLIP data can provide key mechanistic insight into RBP function by revealing positional specificity of RBP binding. Analysis of ZMAT3 binding indicated a remarkable stereotypical positioning, centered 95 nt upstream of 3' splice sites and 30–50 nt upstream of the branch point in the majority of bound transcripts (Figures 6F–6H). Strikingly, this profile of ZMAT3 peaks is distinct from 150 RBPs profiled by the ENCODE consortium (Figures 6G and S6C). For example, maximal ZMAT3 peak density was detected upstream of annotated spliceosomal components, including the 3' splice site factor U2AF2, which binds at the polypyrimidine tract, and branch point factors SF3B4 and RBM5 (Figures 6G and 6H). Moreover, alternative splicing regulatory RBPs PTBP1 and KHSRP, which also bind 100 nt upstream of the 3' splice site, had far broader peak distributions and significant enrichment in 5' splice site regions (Figure 6H). HOMER motif analysis revealed that a subset of the ZMAT3 peaks contain a CAG just 5' of a polypyrimidine tract, reminiscent of the 3' splice site consensus sequence (Figure S6D).

The ZMAT3 binding position, along with the enrichment of genes involved in mRNA splicing in the ZMAT3-bound and regulated transcripts (Figures 6B, 6D, and 6E), suggested that ZMAT3 might regulate splicing. Using rMATS analysis (Park et al., 2013) to compare splice variants in our RNA-seq data from ZMAT3-deficient and control MEFs, we identified 719 ZMAT3-dependent alternative splicing events. The majority of the alternative splicing events were skipped exon (SE) events, but we also found other types of alternative splicing events (Figure 6I; Table S6). Through this analysis, we identified alternative splicing events adjacent to ZMAT3-bound introns, including in transcripts encoding proteins involved in splicing (*Hrrnpd1* and *Dhx9*), p53 regulation (*Mdm4* and *Mdm2*), and varied additional cellular functions (*Dst*, *Sptan1*, and *Bin1*) (Kemmerer et al.,

(C) tdTomato expression in Lenti-sgNC/Cre or Lenti-sgp53/Cre mouse lungs.

(D) Left: sizes of Lenti-sgp53/Cre and Lenti-sgNC/Cre tumors (n = 4 mice/group; n = 160 NC and 193 sgp53 tumors). Each dot represents a tumor, with area proportional to the tumor size. The bar is the mean, and p values, two-tailed unpaired t test. Right: representative H&E-stained lung sections.

(E) tdTomato expression in Lenti-sgNC/Cre or Lenti-sgZmat3/Cre mouse lungs.

(F) Left: sizes of Lenti-sgZmat3/Cre and Lenti-sgNC/Cre tumors (n = 16–20 mice/group; n = 546 negative control and 1,059 sgZmat3 tumors). See plot description in (D). Right: representative H&E-stained lung sections.

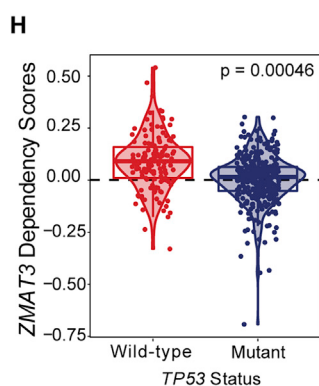
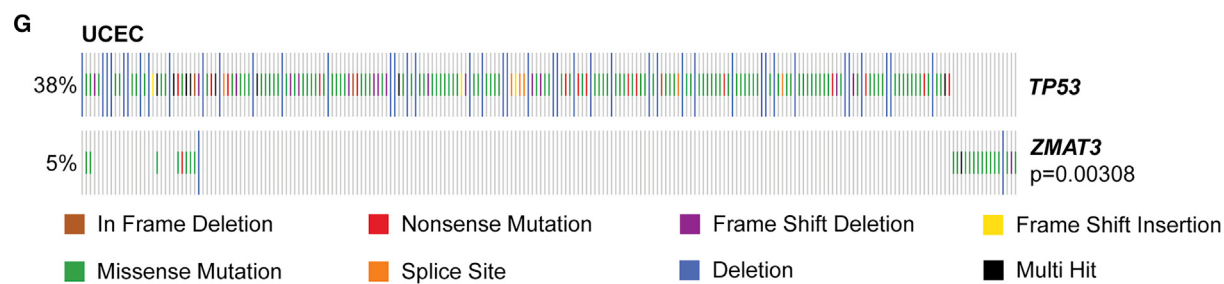
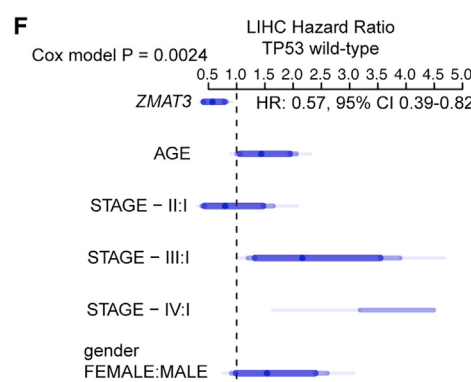
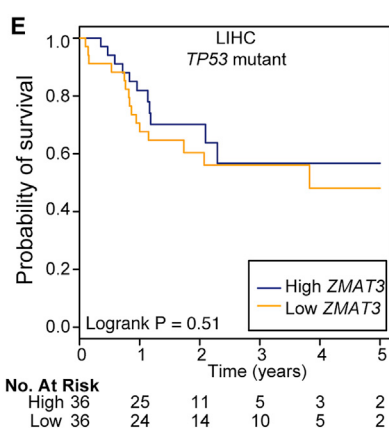
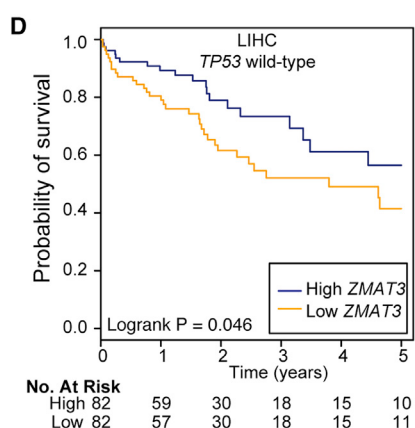
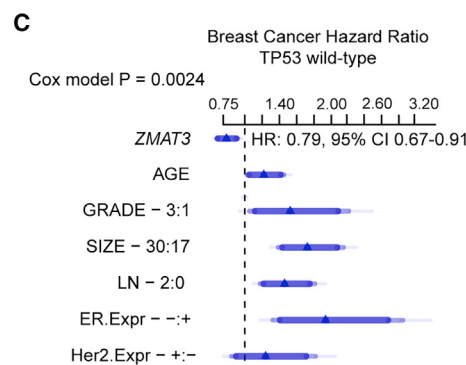
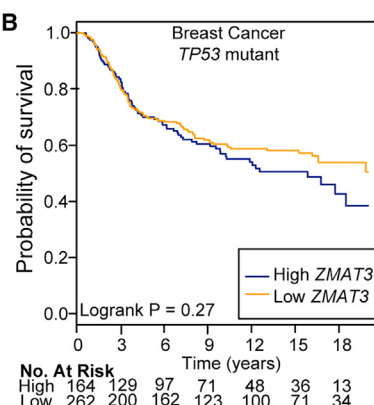
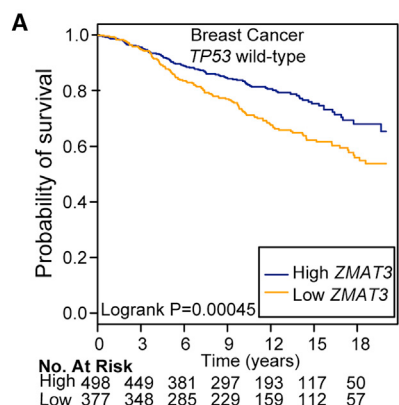
(G and H) Total tumor burden (percentage of tumor area/total lung area) for Lenti-sgp53/Cre and Lenti-sgNC/Cre mice (G, n = 4 sgNC mice, 4 sgp53 mice) and Lenti-sgZmat3/Cre and Lenti-sgNC/Cre mice (H, n = 16 sgNC mice, 20 sgZmat3 mice). Average ± SEM is shown, and each dot represents a mouse. p values, two-tailed unpaired t test.

(I and J) Left: percentages of Ki67-positive nuclei in Lenti-sgp53/Cre and Lenti-sgNC/Cre tumors (I) and Lenti-sgZmat3/Cre and Lenti-sgNC/Cre tumors (J). Right: representative IHC for Ki67 in tumors (n = 20–45 tumors/group). Average ± SEM is shown, and each dot represents a tumor. p values, two-tailed unpaired t test.

(K) Hydrodynamic tail vein injection delivered Sleeping Beauty transposase, *Kras*^{G12D}, and Cas9 + NC sgRNAs (Chrom8), p53 sgRNAs, or either of two different *Zmat3* sgRNAs to mouse livers. Livers were harvested after 7–9 weeks (sgp53) or 14 weeks (sgChrom8 and sgZmat3).

(L and M) Number of tumors per liver (L) and largest tumor diameter (M) in mice injected with sgChrom8, sgp53, or sgZmat3. Average ± SEM is shown, and each dot is a mouse (n = 5 mice/group). p values, two-tailed unpaired t test.

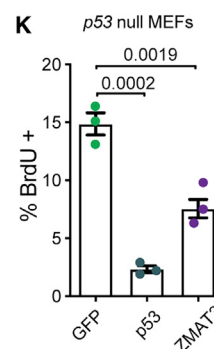
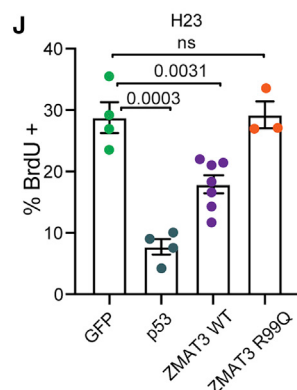
(N) H&E of representative liver tumors or normal liver for sgChrom8.



I

ZMAT3 Co-dependencies:

Gene	Correlation
MDM4	-0.227
TP53BP1	0.224
TP53	0.223
PPM1D	-0.223



(legend on next page)

2018; Künzli et al., 2016; Lee and Pelletier, 2016; Marine et al., 2006; Sakamuro et al., 1996; Wang et al., 2018) (Figure 6J). Interestingly, splicing map analysis did not reveal a consistent pattern of ZMAT3 binding across all ZMAT3-regulated differentially spliced exons (Figure S6E), and numerous alternatively spliced RNAs did not show ZMAT3 binding (e.g., *Cask* and *Tia1*), suggesting that ZMAT3 not only exerts direct effects on splicing, but also indirect downstream effects.

ZMAT3 Regulates Splicing of Transcripts Involved in Diverse Cellular Processes

Of the significant ZMAT3-bound and alternatively spliced transcripts we identified, the p53 negative regulator *Mdm4* is most prominent (Figure 6J). Interestingly, our data show that *Zmat3* knockout cells are enriched for the full-length isoform of *Mdm4* (*Mdm4-FL*), encoding the form that negatively regulates p53 by either directly blocking p53 transactivation or cooperating with the ubiquitin ligase MDM2 to promote p53 degradation (Marine et al., 2006; Toledo and Wahl, 2006) (Figures 7A–7C). In contrast, the ZMAT3-expressing cells also express a short isoform of *Mdm4* (*Mdm4-S*) in which exon 6 is skipped, an event known to introduce a premature termination codon and trigger nonsense-mediated mRNA decay (NMD) (Bardot et al., 2015) (Figures 7A–7C). Therefore, the *Mdm4-S* transcript does not lead to stable MDM4 protein expression, and indeed, we observe less MDM4 protein in ZMAT3-expressing cells than in ZMAT3-deficient cells (Figure 7D). Notably, we also observe a decrease in *Mdm4-S* levels in p53-deficient cells and in cells in which the p53 RE in *Zmat3* is disrupted, suggesting that p53 activation of *Zmat3* is required for the *Mdm4* alternative splicing event (Figure 7D). Exclusion of exon 3 of *Mdm2*, an exon necessary for efficient binding to p53, is also significantly greater in the presence of *Zmat3* (Figures 7A and 7B) (Giglio et al., 2010; Perry et al., 2000). Although p53 protein accumulation is not clearly decreased by *Zmat3* deficiency, expression of some p53 target genes, including *Gtse1* and *Eif4g3*, is diminished (Figures 3I, S6B, and S7A). Thus, these data suggest that one component of *Zmat3* tumor suppressor function is to promote full p53 activity, but it does not fully account for ZMAT3 function, as ZMAT3 clearly can impede proliferation in the absence of p53 (Figures 5J and 5K).

Various other transcripts are bound and alternatively spliced by ZMAT3 (Figure 6J), including splicing regulators, such as *Hnmpd1*—an hnRNP family member involved in alternative

splicing (Kemmerer et al., 2018)—and *Dhx9*—an RNA helicase that interacts with other splicing factors in pre-spliceosomes (Lee and Pelletier, 2016). Both transcripts are bound by ZMAT3 upstream of a 3' splice site adjacent to alternatively spliced exons that are preferentially excluded in ZMAT3-expressing cells (Figures 7E, S7B, S7C, and S7E). The excluded exon in *Hnmpd1* can trigger NMD and transcript destabilization (Kemmerer et al., 2018), consistent with accumulation of this transcript in the presence of ZMAT3. *Dhx9* transcript levels are also increased in ZMAT3-expressing cells (Figure S7B; Table S5), further suggesting that differential splicing could affect transcript stability. By binding transcripts encoding splicing regulators, ZMAT3 may indirectly regulate additional splicing events. ZMAT3 binding also affects splicing of RNAs encoding proteins with roles in various cellular processes, including adhesion, cytoskeletal function, and polarity (*Dst*, *Sptan*, *Dlg1*; Figures 7E, 6J, S7D, and S7E). Collectively, our findings show that ZMAT3 drives alternative splicing of transcripts involved in functionally distinct processes.

ZMAT3 Binds NMD Target Transcripts

Alternative splicing has been reported to trigger NMD in ~30% of alternatively spliced transcripts (Lewis et al., 2003), prompting us to examine whether ZMAT3 preferentially regulates alternative splicing of known NMD targets. We compared the ZMAT3-bound transcripts with alternatively spliced transcripts from RNA-seq analysis of MEFs deficient in SMG1, a kinase that phosphorylates UPF1, a key regulator of NMD (McIlwain et al., 2010). Indeed, ZMAT3 preferentially binds introns flanking SMG1-regulated premature termination codon (PTC)-containing exons relative to non-SMG1 regulated PTC exons or random exons (Figure 7F; see STAR Methods). Thus, at least a subset of ZMAT3 binding occurs on established splicing-regulated NMD targets, supporting the notion that ZMAT3 affects RNA stability through its ability to regulate alternative splicing. Interestingly, analysis of our RNA-seq data revealed that expression of ZMAT3 resulted in significantly higher levels of transcripts bound by ZMAT3 but not all expressed transcripts, suggesting that ZMAT3 binding generally stabilizes mRNAs (Figure 7G).

Collectively, our findings support a model in which ZMAT3 binds transcripts upstream of 3' splice sites, regulates splicing to affect both isoform expression and NMD, and broadly influences gene expression programs. In addition, ZMAT3 action triggers indirect, downstream splicing events. Importantly, given

Figure 5. ZMAT3 Has p53-Dependent and -Independent Activities

- (A and B) Probability of disease-specific survival (DSS) in METABRIC breast cancer patients with wild-type TP53 (A) or mutant TP53 (B) and high (first tertile) or low (third tertile) expression of ZMAT3.
- (C) Cox proportional hazard ratio plot for DSS and ZMAT3 expression levels adjusted for age, grade, size, stage, and estrogen receptor (ER) and HER2 status in METABRIC. Cox proportional hazard p value for ZMAT3 expression: p value: 0.0024, HR: 0.7878, CI 95% 0.67–0.91.
- (D and E) Probability of survival in TCGA LIHC patients with wild-type TP53 (D) or mutant TP53 (E) and high (first tertile) or low (third tertile) expression of ZMAT3.
- (F) Cox proportional hazard ratio plot of the association between survival and ZMAT3 expression levels adjusted for age, stage, and gender in the TCGA LIHC dataset. Cox proportional hazard p value for ZMAT3 expression: p value: 0.0024, HR: 0.57, CI 95% 0.39–0.82.
- (G) Mutations in ZMAT3 are mutually exclusive with TP53 mutations in UCEC. p value, DISCOVER mutual exclusivity test.
- (H) Project Achilles cell lines were parsed on TP53 status (wild type or aberrant) and the CERES dependency score for ZMAT3 plotted for each. p value, Benjamini-Hochberg two-tailed t test.
- (I) Top co-dependencies for ZMAT3 in the CRISPR (Avana) Public 19Q4 dataset with Pearson correlations from DepMap.
- (J and K) H23 cells (J) or p53 null MEFs (K) expressing HA-tagged GFP, p53, wild-type ZMAT3, or ZMAT3 R99Q were analyzed for BrdU incorporation by immunofluorescence. Average ± SEM is shown, and each dot represents a replicate (~200 cells counted per replicate). p values, two-tailed t test.

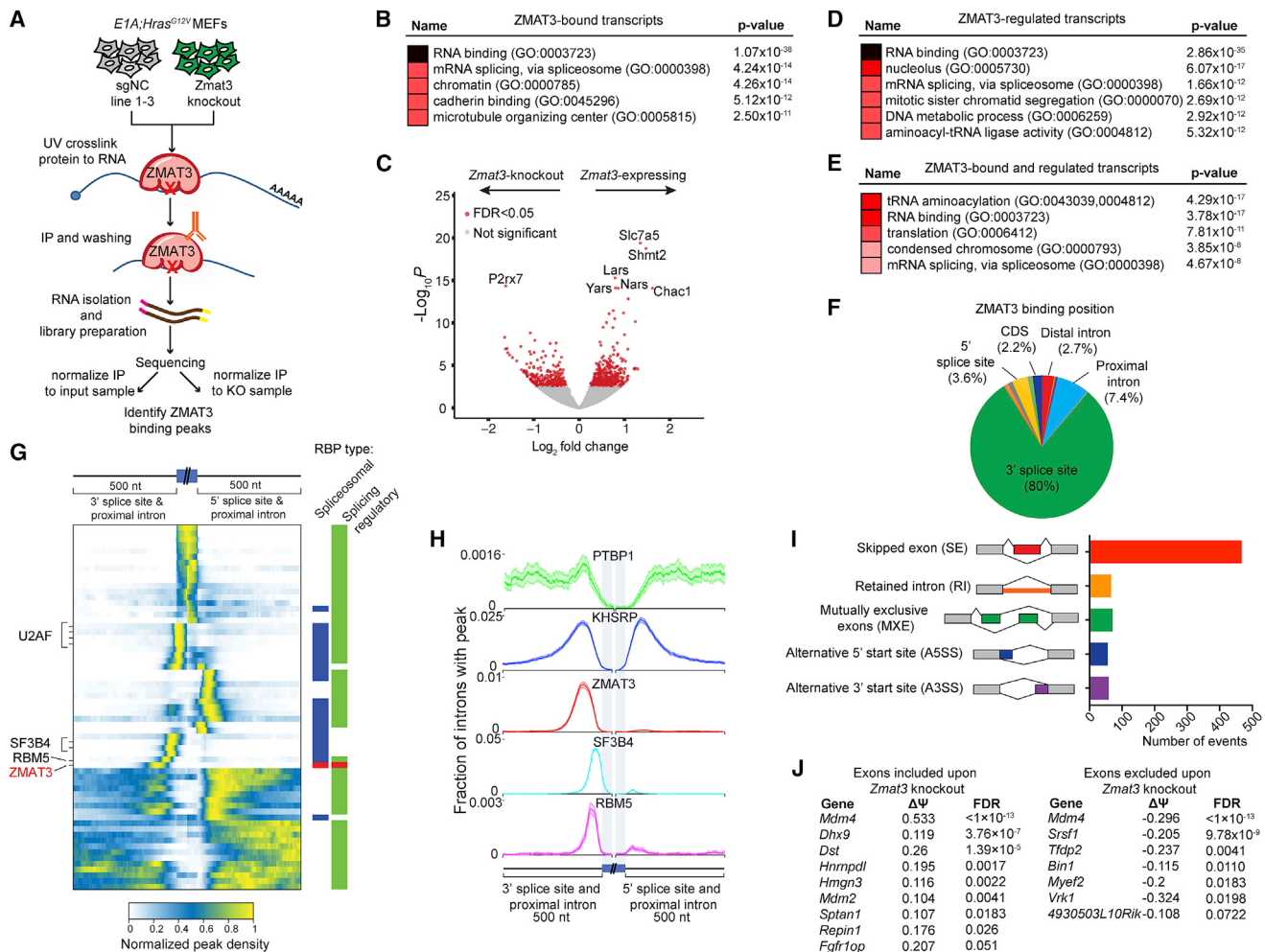


Figure 6. ZMAT3 Is Uniquely Positioned near the 3' Splice Site and Drives Alternative Splicing

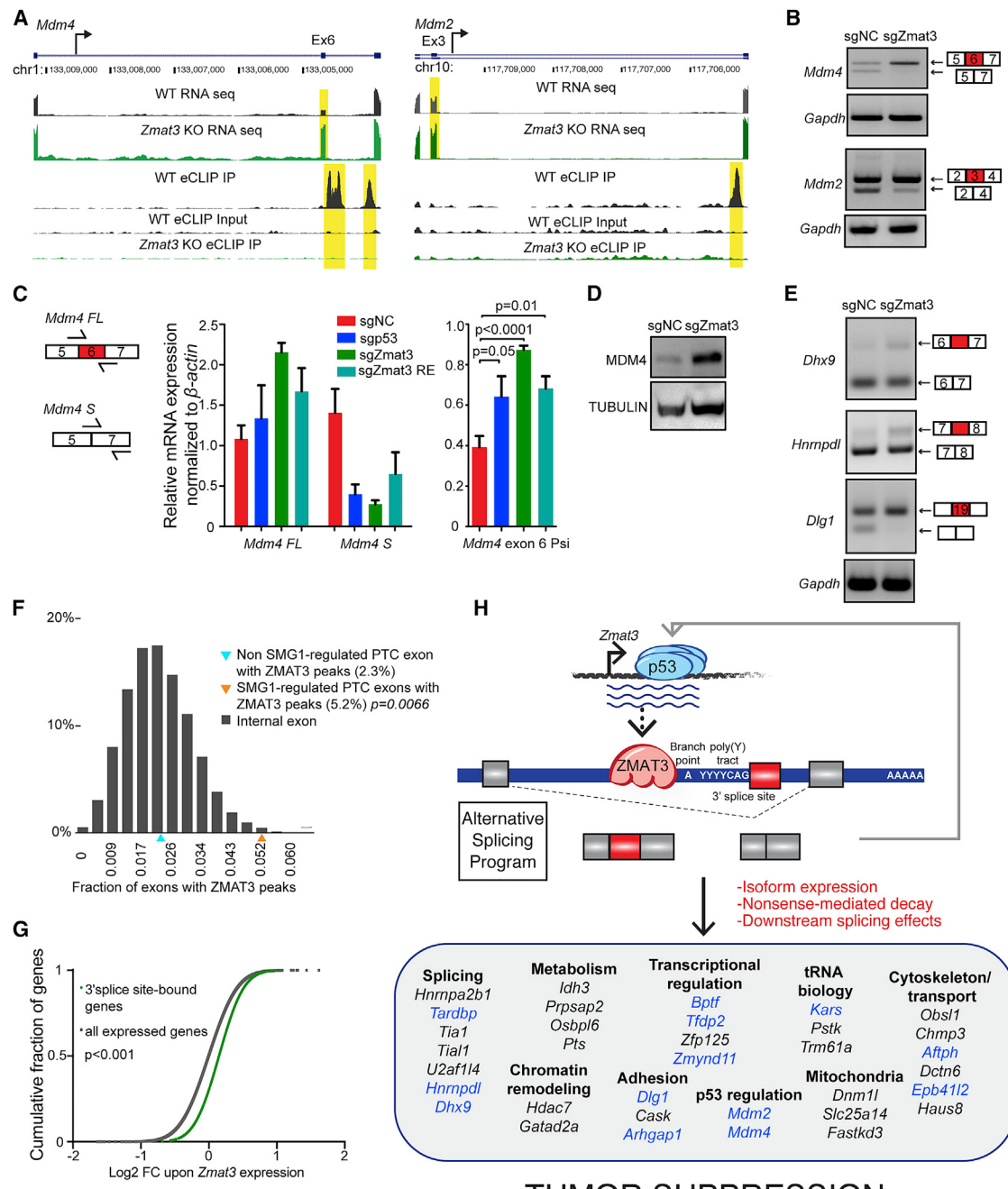
- (A) Schematic for eCLIP experiment.
- (B) Enrichr analysis of top GO terms for the 825 unique transcripts with eCLIP ZMAT3 binding peaks by both input and knockout normalization.
- (C) Volcano plot of 847 differentially expressed genes identified by RNA-seq in *E1A;Hras^{G12V}* MEFs expressing Zmat3 or NC sgRNAs, adjusted p value < 0.05 (red dots).
- (D and E) Enrichr analysis of top GO terms for the 847 genes identified by RNA-seq (D) or the 95 genes on both the RNA-seq and eCLIP gene lists (E).
- (F) Percentage of eCLIP peaks positioned at the indicated locations of the bound RNA in sgNC sample 2 normalized to input and knockout samples.
- (G) Peak density heatmap for ZMAT3 and other spliceosomal components and splicing regulators profiled by CLIP for ENCODE across a meta-mRNA splice junction. Profiles for specific RBPs are marked. Multiple rows for U2AF1 are different cell lines. Right bars mark spliceosomal RBPs (blue), splicing regulatory RBPs (green), and ZMAT3 (red).
- (H) Fraction of introns with a ZMAT3 or other RBP peak across a meta-mRNA splice junction. Shaded regions indicate 5th to 95th percentile from 100 random samplings with replacement.
- (I) rMATS analysis of RNA-seq data from *E1A;Hras^{G12V}* MEFs expressing sgZmat3 or sgNC identifies 719 differential alternative splicing events of different types.
- (J) ZMAT3-dependent alternative splicing events at exons adjacent to ZMAT3 binding in ZMAT3-bound transcripts.

the range of transcripts either differentially expressed or alternatively spliced in the presence of ZMAT3, our findings suggest that the tumor suppressive effect of ZMAT3 is not likely to be explained by a particular bound or alternatively spliced target, but rather through a more complex impact impinging upon diverse cellular pathways (Figure 7H). These findings are in line with previous studies demonstrating that the oncogenic effects of mutations in splicing factors such as SF3B3 and SRSF2 are attributable to subtle splicing changes in a range of transcripts rather

than dramatic changes in splicing of a single transcript (Wang et al., 2016; Zhang et al., 2015).

DISCUSSION

Here, we use a multidisciplinary approach to illuminate p53 transcriptional programs critical for p53 tumor suppressor function. By coupling unbiased ultracomplex RNAi and CRISPR-Cas9 pooled screens *in vivo*, CRISPR-Cas9-mediated genome editing

**Figure 7. Multifaceted Regulation of RNA Splicing and Stability by ZMAT3**

- (A) Alternatively spliced exons (yellow) from the RNA-seq data (upper tracks) and ZMAT3-binding peaks (yellow) from the eCLIP data (lower tracks) in *Mdm4* and *Mdm2*.
- (B) Semiquantitative PCR analysis of the alternative splicing depicted in (A), with *Gapdh* control. Primers were designed to flank the alternatively spliced exon.
- (C) qRT-PCR analysis of *Mdm4* exon 6 alternative splicing (mean \pm SD) in *E1A;Hras^{G12V}*;Cas9 MEFs transduced with sgRNAs targeting Zmat3, p53, the Zmat3 p53 RE, or NC sgRNAs, relative to β -actin. *p* value, two-tailed unpaired *t* test of different MEF lines ($n = 3\text{--}8$).
- (D) Western blot analysis of MDM4 in *E1A;Hras^{G12V}*;Cas9 MEFs expressing sgZmat3 or sgNC with α -TUBULIN loading control.
- (E) Semiquantitative PCR analysis of alternative splicing in *Dhx9*, *Hnmpdl*, and *Dlg1* with *Gapdh* control. Primers were designed to flank the alternatively spliced exons.
- (F) Frequency of ZMAT3 binding peaks flanking SMG1-dependent exons (orange triangle), non SMG1-dependent exons (blue triangle), or random exons (gray bars). Significance based on comparison to random exons.

(legend continued on next page)

in autochthonous mouse cancer models, human cancer genome analysis, and integrative eCLIP-seq and RNA-seq analyses, we reveal an important branch of p53 tumor suppression involving an RNA splicing program. While recent studies have underscored the importance of dysregulated splicing for cancer development (Obeng et al., 2019; Zhang and Manley, 2013) and suggested a role for mutant p53 in regulating splicing in pancreas cancer (Escobar-Hoyos et al., 2020), a clear link to wild-type p53 has not been established. We show further that ZMAT3 is most active in the context of an intact p53 pathway and that ZMAT3 controls p53 regulators, suggesting that feedback to p53 may account for some ZMAT3 tumor suppressor activity. However, ZMAT3 expression is sufficient to inhibit proliferation in p53-deficient cells, indicating that ZMAT3 can also employ p53-independent tumor suppressive mechanisms. Interestingly, a recent shRNA screen revealed that *Zmat3* knockdown in hematopoietic stem cells deficient for the p53 target genes *Puma* and *p21* promotes leukemia development (Janic et al., 2018). Together with our data revealing a tumor suppressor role for *Zmat3* in *E1A;Hras^{G12V}* MEFs, LUAD, and HCC, these observations support the idea that ZMAT3 represents a core component of p53 tumor suppression across various contexts.

Although *ZMAT3* has been known as a p53 target gene for some time (Israeli et al., 1997; Varmeh-Ziaie et al., 1997), its physiological function and role in tumor suppression are not well understood. Previous studies have suggested that ZMAT3 is a double-stranded RBP that binds 3' UTRs of various mRNAs to modulate RNA levels (Bersani et al., 2014, 2016; Vilborg et al., 2009). Here, we used the highly sensitive eCLIP technique (Van Nostrand et al., 2016), coupled with RNA-seq, to understand ZMAT3 function. We identified hundreds of novel ZMAT3-bound transcripts, but only ~1% of ZMAT3 binding events were at the 3' UTR. Instead, we observed dramatic enrichment of ZMAT3 binding upstream of the 3' splice site of specific introns in the majority of transcripts, strongly suggesting that ZMAT3 functions to regulate splicing. Indeed, we observed ZMAT3-dependent regulation of alternative splicing of numerous transcripts. Notably, *Zmat3* knockout affects splicing of select transcripts, suggesting that ZMAT3 is a regulator of alternative splicing rather than being a core splicing component. Intriguingly, we noted multiple instances of known “poison exons”—regulated alternatively spliced exons containing stop codons that trigger NMD (Kurosaki et al., 2019). Depending on whether these exons are included or excluded, transcripts may be stabilized or destabilized by ZMAT3. Thus, there may be additional ZMAT3-regulated alternative splicing events that we failed to detect in our RNA-seq due to degradation of the alternative isoform.

Inclusion of cryptic exons—nonannotated exons defined by sequences similar to consensus motifs of canonical splice sites—occurs in human disease and can also trigger NMD (Sibley et al., 2016; Ule and Blencowe, 2019). Recent studies have suggested that suppression of cryptic splice site recognition is a key function of some RBPs, such as the ZMAT3-related protein

MATRIN 3, which binds and blocks the use of cryptic splice sites in antisense LINE elements (Attig et al., 2018). As with MATRIN3, ZMAT3 knockdown causes a small but significant decrease in ZMAT3-bound transcript levels. Although we do not yet know the mechanism by which ZMAT3 recognizes its specific targets, motif enrichment analysis revealed ZMAT3 binding to sequences resembling the consensus 3' splice site (CAG + polypyrimidine tract). Thus, ZMAT3 may maintain proper expression of its targets by suppressing the use of specific cryptic alternative 3' splice sites.

The direct modulation of alternative splicing by ZMAT3 promotes alterations in the expression of genes involved in p53 regulation, various cellular processes, and splicing itself. Notably, we do not observe splicing changes in the *Trp53* transcript (Figure S7F). The most dramatic effect is on the p53 inhibitor MDM4, for which different spliced isoforms have been described, including those expressing and lacking exon 6 (Bardot et al., 2015; Boutz et al., 2015). Critical evidence for the functional roles of the isoforms has come, in part, from mice expressing an *Mdm4* allele lacking exon 6, which display embryonic lethality provoked by diminished *Mdm4* expression and inappropriate p53 activation (Bardot et al., 2015). Moreover, inhibition of exon 6 inclusion using antisense oligonucleotides impairs melanoma growth *in vivo* (Dewaele et al., 2016). Thus, the main function of the alternative splicing event in *Mdm4* that drives exon 6 skipping is to reduce the amount of full-length *Mdm4* produced and promote active p53. While specific regulators of splicing, such as SRSF proteins and PRMT5, have been genetically defined as modulators of *Mdm4* exon 6 skipping (Dewaele et al., 2016; Fong et al., 2019), we propose that ZMAT3 binding to RNA directly dictates the occurrence of this event, as a means to maintain p53 activity.

Beyond driving this specific alternative splicing event, ZMAT3 likely impedes tumor development through combined effects on the various transcripts that it binds and directly regulates. Interestingly, ZMAT3 regulates splicing of transcripts encoding proteins involved in diverse cellular processes. For example, DST is a hemidesmosome component involved in epithelial cell–basement membrane adhesion (Künzli et al., 2016), DLG1 is a cell polarity/signaling protein originally identified from a *Drosophila* larva overgrowth phenotype (Milgrom-Hoffman and Humbert, 2018), and SPTAN1 is a cytoskeletal scaffold protein (Ackermann and Brieger, 2019). Therefore, ZMAT3 regulation of such transcripts, by modulating isoform expression or levels, may influence tumorigenesis. In addition, our finding that some ZMAT3-bound and differentially spliced genes are themselves splicing regulators suggests that ZMAT3 also indirectly impinges on the alternative splicing of a broad network of transcripts. Indeed, rMATS analysis reveals hundreds of transcripts not clearly bound by ZMAT3 but nonetheless alternatively spliced in a ZMAT3-dependent fashion. Interestingly, these RNAs are involved in a wide range of cellular processes, suggesting how ZMAT3 could contribute to tumor suppression in a pleiotropic fashion.

Beyond *Zmat3*, our screening platform identified other tumor suppressor genes. *Dennd2c* is a member of the DENN domain

(G) Cumulative distribution plots of gene expression fold change (\log_2) for transcripts bound by ZMAT3 near a 3' splice site (green line) or all expressed genes (gray line) in the RNA-seq data. $p < 0.001$, Kolmogorov-Smirnov test.

(H) Model for ZMAT3 action in tumor suppression. Transcripts in blue are ZMAT3 bound in eCLIP data, those in black are not bound, based on statistics.

family of proteins that act as Rab-GEFs and regulate intracellular trafficking (Yoshimura et al., 2010). While not well studied, DENND2C may regulate autophagy, a process modulated by p53 and sometimes involved in tumor suppression (Jung et al., 2017; Kenzelmann Broz et al., 2013). The identification of *Ptpn14*, which we have shown suppresses both YAP and pancreatic cancer (Mello et al., 2017), as well as *Trp53inp1*, *Ldhb*, and *Gss*, which all encode metabolic regulators, highlights additional pathways that likely contribute to p53-mediated tumor suppression. The identification of such novel functional tumor suppressor genes is critical for helping to deconvolute human cancer genome sequencing data by unveiling genes with tumor suppressor activity and is a first step toward delineating the cooperating p53 programs involved in suppressing cancer. Ultimately, deconstructing the pathways through which p53 acts may lead to new opportunities for therapeutic intervention in cancer.

STAR METHODS

Detailed methods are provided in the online version of this paper and include the following:

- **KEY RESOURCES TABLE**
- **RESOURCE AVAILABILITY**
 - Lead Contact
 - Materials Availability
 - Data and Code Availability
- **EXPERIMENTAL MODEL AND SUBJECT DETAILS**
 - Subcutaneous tumor model
 - Mouse lung adenocarcinoma study
 - Mouse HCC study
 - Mouse cell culture and viral infections
 - Human cell culture
- **METHOD DETAILS**
 - TSAG identification
 - Library design, amplification, and sequencing
 - Analysis of shRNA library screens
 - Analysis of CRISPR-Cas9 library screens
 - Transformation assays
 - *In vivo* competition assay
 - Analysis of CRISPR indels
 - qRT-PCR and Semiquantitative PCR
 - ChIP
 - Western blots
 - Immunohistochemistry
 - Overexpression and immunofluorescence
 - Human cancer data analysis
 - ZMAT3 eCLIP and data analysis
 - RNA-seq
 - RNA-seq alternative splicing analysis
 - Comparing ZMAT3 peaks and SMG1-regulated exons
 - Analysis of DepMap samples
- **QUANTIFICATION AND STATISTICAL ANALYSIS**

SUPPLEMENTAL INFORMATION

Supplemental Information can be found online at <https://doi.org/10.1016/j.molcel.2020.10.022>.

ACKNOWLEDGMENTS

We thank Laurakay Bruhn, Steven Altschuler, Ben Borgo, Peter Sheffield, and Carsten Carstens of Agilent Inc. for oligonucleotide synthesis and helpful discussions. We thank Lin He for the *E μ -Myc* lymphoma cells, Andreas Strasser and Ana Janic for the *Zmat3* null MEFs, and Julien Sage and Aaron Gitler for critical reading of the manuscript. This work was supported by NIH R35 grant CA197591 and Tobacco-Related Disease Research Program grant 28IP-0037 to L.D.A. and an American Cancer Society Postdoctoral Fellowship PF-12-195-01-TGB and National Research Service Award F32 CA162681-02 to K.T.B.-R.

AUTHOR CONTRIBUTIONS

K.T.B.-R. designed and performed experiments, interpreted data, and wrote the manuscript. A.K. and A.M.B. designed and performed experiments and analyzed data. D.W.M. and M.C.B. designed shRNA and sgRNA libraries and interpreted the screen results. J.A.S. and C.C. performed human tumor analyses. S.S.M. performed TSAG identification and RNA-seq analyses. J.M. performed western blots. M.W. generated the *Zmat3* R99Q construct. C.Z., S.L.H., and S.W.L. designed, performed, and analyzed mouse HCC experiments. E.L.V.N., B.A.Y., and G.W.Y. performed, analyzed, and interpreted ZMAT3 eCLIP and splicing experiments. I.P.W. and M.M.W. assisted with mouse Lenti/Cre LUAD experiments. S.E.P. performed dependency score analysis. A.J.C. assisted with mouse lung histological analyses. L.D.A. designed experiments, interpreted data, and wrote the manuscript.

DECLARATION OF INTERESTS

E.L.V.N. is cofounder, member of the Board of Directors, on the scientific advisory board, equity holder, and paid consultant for Eclipse BioInnovations. G.W.Y. is cofounder, member of the Board of Directors, on the scientific advisory board, equity holder, and paid consultant for Locana and Eclipse BioInnovations. G.W.Y. is a visiting professor at the National University of Singapore. Dr. Yeo's interest(s) have been reviewed and approved by UCSD in accordance with its conflict of interest policies. S.W.L. is a member of the scientific advisory board of PMV Pharmaceuticals. The authors declare no other competing financial interests.

Received: February 13, 2020

Revised: August 19, 2020

Accepted: October 14, 2020

Published: November 5, 2020

REFERENCES

- Ackermann, A., and Brieger, A. (2019). The Role of Nonerythroid Spectrin α II in Cancer. *J. Oncol.* 2019, 7079604.
- Afghan, E., Baker, D., Batut, B., van den Beek, M., Bouvier, D., Cech, M., Chilton, J., Clements, D., Coraor, N., Grüning, B.A., et al. (2018). The Galaxy platform for accessible, reproducible and collaborative biomedical analyses: 2018 update. *Nucleic Acids Res.* 46 (W1), W537–W544.
- Al Saati, T., Clerc, P., Hanoun, N., Peugnet, S., Lulka, H., Gigoux, V., Capilla, F., Béluchon, B., Couvelard, A., Selves, J., et al. (2013). Oxidative stress induced by inactivation of TP53INP1 cooperates with KrasG12D to initiate and promote pancreatic carcinogenesis in the murine pancreas. *Am. J. Pathol.* 182, 1996–2004.
- Andrysiak, Z., Galbraith, M.D., Guarnieri, A.L., Zaccara, S., Sullivan, K.D., Pandey, A., MacBeth, M., Inga, A., and Espinosa, J.M. (2017). Identification of a core TP53 transcriptional program with highly distributed tumor suppressive activity. *Genome Res.* 27, 1645–1657.
- Attig, J., Agostini, F., Gooding, C., Chakrabarti, A.M., Zaccara, S., Sullivan, K.D., Zagalak, J.A., Emmett, W., Smith, C.W.J., Luscombe, N.M., and Ule, J. (2018). Heteromeric RNP Assembly at LINEs Controls Lineage-Specific RNA Processing. *Cell* 174, 1067–1081.e17.

- Bardot, B., Bouarch-Bourimi, R., Leempt, J., Lejour, V., Hamon, A., Plancke, L., Jochemsen, A.G., Simeonova, I., Fang, M., and Toledo, F. (2015). Mice engineered for an obligatory Mdm4 exon skipping express higher levels of the Mdm4-S isoform but exhibit increased p53 activity. *Oncogene* 34, 2943–2948.
- Bassik, M.C., Lebbink, R.J., Churchman, L.S., Ingolia, N.T., Patena, W., LeProust, E.M., Schuldiner, M., Weissman, J.S., and McManus, M.T. (2009). Rapid creation and quantitative monitoring of high coverage shRNA libraries. *Nat. Methods* 6, 443–445.
- Bersani, C., Xu, L.D., Vilborg, A., Lui, W.O., and Wiman, K.G. (2014). Wig-1 regulates cell cycle arrest and cell death through the p53 targets FAS and 14-3- σ . *Oncogene* 33, 4407–4417.
- Bersani, C., Huss, M., Giacomello, S., Xu, L.D., Bianchi, J., Eriksson, S., Jerhammar, F., Alexeyenko, A., Vilborg, A., Lundeberg, J., et al. (2016). Genome-wide identification of Wig-1 mRNA targets by RIP-Seq analysis. *Oncotarget* 7, 1895–1911.
- Bieging, K.T., Mello, S.S., and Attardi, L.D. (2014). Unravelling mechanisms of p53-mediated tumour suppression. *Nat. Rev. Cancer* 14, 359–370.
- Boutz, P.L., Bhutkar, A., and Sharp, P.A. (2015). Detained introns are a novel, widespread class of post-transcriptionally spliced introns. *Genes Dev.* 29, 63–80.
- Bowen, M.E., McClendon, J., Long, H.K., Soraya, A., Van Nostrand, J.L., Wysocka, J., and Attardi, L.D. (2019). The Spatiotemporal Pattern and Intensity of p53 Activation Dictates Phenotypic Diversity in p53-Driven Developmental Syndromes. *Dev. Cell* 50, 212–228.e6.
- Brady, C.A., Jiang, D., Mello, S.S., Johnson, T.M., Jarvis, L.A., Kozak, M.M., Kenzelmann Broz, D., Basak, S., Park, E.J., McLaughlin, M.E., et al. (2011). Distinct p53 transcriptional programs dictate acute DNA-damage responses and tumor suppression. *Cell* 145, 571–583.
- Canisius, S., Martens, J.W., and Wessels, L.F. (2016). A novel independence test for somatic alterations in cancer shows that biology drives mutual exclusivity but chance explains most co-occurrence. *Genome Biol.* 17, 261.
- Cano, C.E., Gommeaux, J., Pietri, S., Culcasi, M., Garcia, S., Seux, M., Barelier, S., Vasseur, S., Spoto, R.P., Pébusque, M.J., et al. (2009). Tumor protein 53-induced nuclear protein 1 is a major mediator of p53 antioxidant function. *Cancer Res.* 69, 219–226.
- Cerami, E., Gao, J., Dogrusoz, U., Gross, B.E., Sumer, S.O., Aksoy, B.A., Jacobsen, A., Byrne, C.J., Heuer, M.L., Larsson, E., et al. (2012). The cBio cancer genomics portal: an open platform for exploring multidimensional cancer genomics data. *Cancer Discov.* 2, 401–404.
- Chiou, S.H., Winters, I.P., Wang, J., Naranjo, S., Dudgeon, C., Tamburini, F.B., Brady, J.J., Yang, D., Grüner, B.M., Chuang, C.H., et al. (2015). Pancreatic cancer modeling using retrograde viral vector delivery and *in vivo* CRISPR/Cas9-mediated somatic genome editing. *Genes Dev.* 29, 1576–1585.
- Christophorou, M.A., Martin-Zanca, D., Soucek, L., Lawlor, E.R., Brown-Swigart, L., Verschuren, E.W., and Evan, G.I. (2005). Temporal dissection of p53 function *in vitro* and *in vivo*. *Nat. Genet.* 37, 718–726.
- Cong, L., Ran, F.A., Cox, D., Lin, S., Barretto, R., Habib, N., Hsu, P.D., Wu, X., Jiang, W., Marraffini, L.A., and Zhang, F. (2013). Multiplex genome engineering using CRISPR/Cas systems. *Science* 339, 819–823.
- Curtis, C., Shah, S.P., Chin, S.F., Turashvili, G., Rueda, O.M., Dunning, M.J., Speed, D., Lynch, A.G., Samarajiva, S., Yuan, Y., et al.; METABRIC Group (2012). The genomic and transcriptomic architecture of 2,000 breast tumours reveals novel subgroups. *Nature* 486, 346–352.
- Deans, R.M., Morgens, D.W., Ökesli, A., Pillay, S., Horlbeck, M.A., Kampmann, M., Gilbert, L.A., Li, A., Mateo, R., Smith, M., et al. (2016). Parallel shRNA and CRISPR-Cas9 screens enable antiviral drug target identification. *Nat. Chem. Biol.* 12, 361–366.
- Dewaele, M., Tabaglio, T., Willekens, K., Bezzi, M., Teo, S.X., Low, D.H., Koh, C.M., Rambow, F., Fiers, M., Rogiers, A., et al. (2016). Antisense oligonucleotide-mediated MDM4 exon 6 skipping impairs tumor growth. *J. Clin. Invest.* 126, 68–84.
- Dobin, A., Davis, C.A., Schlesinger, F., Drenkow, J., Zaleski, C., Jha, S., Batut, P., Chaisson, M., and Gingeras, T.R. (2013). STAR: ultrafast universal RNA-seq aligner. *Bioinformatics* 29, 15–21.
- DuPage, M., Dooley, A.L., and Jacks, T. (2009). Conditional mouse lung cancer models using adenoviral or lentiviral delivery of Cre recombinase. *Nat. Protoc.* 4, 1064–1072.
- Escobar-Hoyos, L.F., Penson, A., Kannan, R., Cho, H., Pan, C.H., Singh, R.K., Apken, L.H., Hobbs, G.A., Luo, R., Lecomte, N., et al. (2020). Altered RNA Splicing by Mutant p53 Activates Oncogenic RAS Signaling in Pancreatic Cancer. *Cancer Cell* 38, 198–211.e8.
- Feldser, D.M., Kostova, K.K., Winslow, M.M., Taylor, S.E., Cashman, C., Whittaker, C.A., Sanchez-Rivera, F.J., Resnick, R., Bronson, R., Hemann, M.T., and Jacks, T. (2010). Stage-specific sensitivity to p53 restoration during lung cancer progression. *Nature* 468, 572–575.
- Fong, J.Y., Pignata, L., Goy, P.A., Kawabata, K.C., Lee, S.C., Koh, C.M., Musiani, D., Massignani, E., Kotini, A.G., Penson, A., et al. (2019). Therapeutic Targeting of RNA Splicing Catalysis through Inhibition of Protein Arginine Methylation. *Cancer Cell* 36, 194–209.e9.
- Gao, J., Aksoy, B.A., Dogrusoz, U., Dresdner, G., Gross, B., Sumer, S.O., Sun, Y., Jacobsen, A., Sinha, R., Larsson, E., et al. (2013). Integrative analysis of complex cancer genomics and clinical profiles using the cBioPortal. *Sci. Signal.* 6, pl1.
- Giglio, S., Mancini, F., Pellegrino, M., Di Conza, G., Puxeddu, E., Sacchi, A., Pontecorvi, A., and Moretti, F. (2010). Regulation of MDM4 (MDMX) function by p76(MDM2): a new facet in the control of p53 activity. *Oncogene* 29, 5935–5945.
- Han, K., Jeng, E.E., Hess, G.T., Morgens, D.W., Li, A., and Bassik, M.C. (2017). Synergistic drug combinations for cancer identified in a CRISPR screen for pairwise genetic interactions. *Nat. Biotechnol.* 35, 463–474.
- Hess, G.T., Frésard, L., Han, K., Lee, C.H., Li, A., Cimprich, K.A., Montgomery, S.B., and Bassik, M.C. (2016). Directed evolution using dCas9-targeted somatic hypermutation in mammalian cells. *Nat. Methods* 13, 1036–1042.
- Huang, C.H., Lujambio, A., Zuber, J., Tschaharganeh, D.F., Doran, M.G., Evans, M.J., Kitzing, T., Zhu, N., de Stanchina, E., Sawyers, C.L., et al. (2014). CDK9-mediated transcription elongation is required for MYC addiction in hepatocellular carcinoma. *Genes Dev.* 28, 1800–1814.
- Israeli, D., Tessler, E., Haupt, Y., Elkeles, A., Wilder, S., Amson, R., Telerman, A., and Oren, M. (1997). A novel p53-inducible gene, PAG608, encodes a nuclear zinc finger protein whose overexpression promotes apoptosis. *EMBO J.* 16, 4384–4392.
- Jackson, E.L., Willis, N., Mercer, K., Bronson, R.T., Crowley, D., Montoya, R., Jacks, T., and Tuveson, D.A. (2001). Analysis of lung tumor initiation and progression using conditional expression of oncogenic K-ras. *Genes Dev.* 15, 3243–3248.
- Janic, A., Valente, L.J., Wakefield, M.J., Di Stefano, L., Milla, L., Wilcox, S., Yang, H., Tai, L., Vandenberg, C.J., Kueh, A.J., et al. (2018). DNA repair processes are critical mediators of p53-dependent tumor suppression. *Nat. Med.* 24, 947–953.
- Jiang, D., Brady, C.A., Johnson, T.M., Lee, E.Y., Park, E.J., Scott, M.P., and Attardi, L.D. (2011). Full p53 transcriptional activation potential is dispensable for tumor suppression in diverse lineages. *Proc. Natl. Acad. Sci. USA* 108, 17123–17128.
- Johnson, L., Mercer, K., Greenbaum, D., Bronson, R.T., Crowley, D., Tuveson, D.A., and Jacks, T. (2001). Somatic activation of the K-ras oncogene causes early onset lung cancer in mice. *Nature* 410, 1111–1116.
- Johnson, J.L., Monfregola, J., Napolitano, G., Kiosses, W.B., and Catz, S.D. (2012). Vesicular trafficking through cortical actin during exocytosis is regulated by the Rab27a effector JFC1/Slp1 and the RhoA-GTPase-activating protein Gem-interacting protein. *Mol. Biol. Cell* 23, 1902–1916.
- Jung, J., Nayak, A., Schaeffer, V., Starzetz, T., Kirsch, A.K., Müller, S., Dikic, I., Mittelbronn, M., and Behrends, C. (2017). Multiplex image-based autophagy RNAi screening identifies SMCR8 as ULK1 kinase activity and gene expression regulator. *eLife* 6, 6.

- Kampmann, M., Horlbeck, M.A., Chen, Y., Tsai, J.C., Bassik, M.C., Gilbert, L.A., Villalta, J.E., Kwon, S.C., Chang, H., Kim, V.N., and Weissman, J.S. (2015). Next-generation libraries for robust RNA interference-based genome-wide screens. *Proc. Natl. Acad. Sci. USA* 112, E3384–E3391.
- Kandoth, C., McLellan, M.D., Vandin, F., Ye, K., Niu, B., Lu, C., Xie, M., Zhang, Q., McMichael, J.F., Wyczalkowski, M.A., et al. (2013). Mutational landscape and significance across 12 major cancer types. *Nature* 502, 333–339.
- Kemmerer, K., Fischer, S., and Weigand, J.E. (2018). Auto- and cross-regulation of the hnRNPs D and DL. *RNA* 24, 324–331.
- Kenzelmann Broz, D., Spano Mello, S., Biegling, K.T., Jiang, D., Dusek, R.L., Brady, C.A., Sidow, A., and Attardi, L.D. (2013). Global genomic profiling reveals an extensive p53-regulated autophagy program contributing to key p53 responses. *Genes Dev.* 27, 1016–1031.
- Kuleshov, M.V., Jones, M.R., Rouillard, A.D., Fernandez, N.F., Duan, Q., Wang, Z., Koplev, S., Jenkins, S.L., Jagodnik, K.M., Lachmann, A., et al. (2016). Enrichr: a comprehensive gene set enrichment analysis web server 2016 update. *Nucleic Acids Res.* 44 (W1), W90–7.
- Künzli, K., Favre, B., Chofflon, M., and Borradori, L. (2016). One gene but different proteins and diseases: the complexity of dystonin and bullous pemphigoid antigen 1. *Exp. Dermatol.* 25, 10–16.
- Kurosaki, T., Popp, M.W., and Maquat, L.E. (2019). Quality and quantity control of gene expression by nonsense-mediated mRNA decay. *Nat. Rev. Mol. Cell Biol.* 20, 406–420.
- Langmead, B., Trapnell, C., Pop, M., and Salzberg, S.L. (2009). Ultrafast and memory-efficient alignment of short DNA sequences to the human genome. *Genome Biol.* 10, R25.
- Lee, T., and Pelletier, J. (2016). The biology of DHX9 and its potential as a therapeutic target. *Oncotarget* 7, 42716–42739.
- Lee, K.H., Li, M., Michalowski, A.M., Zhang, X., Liao, H., Chen, L., Xu, Y., Wu, X., and Huang, J. (2010). A genomewide study identifies the Wnt signaling pathway as a major target of p53 in murine embryonic stem cells. *Proc. Natl. Acad. Sci. USA* 107, 69–74.
- Lewis, B.P., Green, R.E., and Brenner, S.E. (2003). Evidence for the widespread coupling of alternative splicing and nonsense-mediated mRNA decay in humans. *Proc. Natl. Acad. Sci. USA* 100, 189–192.
- Li, M., He, Y., Dubois, W., Wu, X., Shi, J., and Huang, J. (2012a). Distinct regulatory mechanisms and functions for p53-activated and p53-repressed DNA damage response genes in embryonic stem cells. *Mol. Cell* 46, 30–42.
- Li, T., Kon, N., Jiang, L., Tan, M., Ludwig, T., Zhao, Y., Baer, R., and Gu, W. (2012b). Tumor suppression in the absence of p53-mediated cell-cycle arrest, apoptosis, and senescence. *Cell* 149, 1269–1283.
- Liao, Y., Smyth, G.K., and Shi, W. (2014). featureCounts: an efficient general purpose program for assigning sequence reads to genomic features. *Bioinformatics* 30, 923–930.
- Love, M.I., Huber, W., and Anders, S. (2014). Moderated estimation of fold change and dispersion for RNA-seq data with DESeq2. *Genome Biol.* 15, 550.
- Lowe, S.W., Jacks, T., Housman, D.E., and Ruley, H.E. (1994). Abrogation of oncogene-associated apoptosis allows transformation of p53-deficient cells. *Proc. Natl. Acad. Sci. USA* 91, 2026–2030.
- Madisen, L., Zwingman, T.A., Sunkin, S.M., Oh, S.W., Zariwala, H.A., Gu, H., Ng, L.L., Palmiter, R.D., Hawrylycz, M.J., Jones, A.R., et al. (2010). A robust and high-throughput Cre reporting and characterization system for the whole mouse brain. *Nat. Neurosci.* 13, 133–140.
- Marine, J.C., Francoz, S., Maetens, M., Wahl, G., Toledo, F., and Lozano, G. (2006). Keeping p53 in check: essential and synergistic functions of Mdm2 and Mdm4. *Cell Death Differ.* 13, 927–934.
- Martin, M. (2011). Cutadapt Removes Adapter Sequences From High-Throughput Sequencing Reads. *EMBnet.journal* 17, 10–12.
- Mayakonda, A., and Koeffler, H.P. (2016). Maftools: Efficient analysis, visualization, and summarization of MAF files from large-scale cohort based cancer studies. *bioRxiv*. <https://doi.org/10.1101/052662>.
- McIlwain, D.R., Pan, Q., Reilly, P.T., Elia, A.J., McCracken, S., Wakeham, A.C., Itie-Youten, A., Blencowe, B.J., and Mak, T.W. (2010). Smg1 is required for embryogenesis and regulates diverse genes via alternative splicing coupled to nonsense-mediated mRNA decay. *Proc. Natl. Acad. Sci. USA* 107, 12186–12191.
- Mello, S.S., and Attardi, L.D. (2018). Deciphering p53 signaling in tumor suppression. *Curr. Opin. Cell Biol.* 51, 65–72.
- Mello, S.S., Valente, L.J., Raj, N., Seoane, J.A., Flowers, B.M., McClendon, J., Biegling-Rolett, K.T., Lee, J., Ivanochko, D., Kozak, M.M., et al. (2017). A p53 Super-tumor Suppressor Reveals a Tumor Suppressive p53-Ptpn14-Yap Axis in Pancreatic Cancer. *Cancer Cell* 32, 460–473.e6.
- Méndez-Vidal, C., Wilhelm, M.T., Hellborg, F., Qian, W., and Wiman, K.G. (2002). The p53-induced mouse zinc finger protein wig-1 binds double-stranded RNA with high affinity. *Nucleic Acids Res.* 30, 1991–1996.
- Meyers, R.M., Bryan, J.G., McFarland, J.M., Weir, B.A., Sizemore, A.E., Xu, H., Dharia, N.V., Montgomery, P.G., Cowley, G.S., Pantel, S., et al. (2017). Computational correction of copy number effect improves specificity of CRISPR-Cas9 essentiality screens in cancer cells. *Nat. Genet.* 49, 1779–1784.
- Milgrom-Hoffman, M., and Humbert, P.O. (2018). Regulation of cellular and PCP signalling by the Scribble polarity module. *Semin. Cell Dev. Biol.* 81, 33–45.
- Moon, S.H., Huang, C.H., Houlihan, S.L., Regunath, K., Freed-Pastor, W.A., Morris, J.P., 4th, Tschaharganeh, D.F., Kastenhuber, E.R., Barsotti, A.M., Culp-Hill, R., et al. (2019). p53 Represses the Mevalonate Pathway to Mediate Tumor Suppression. *Cell* 176, 564–580.e19.
- Morgens, D.W., Deans, R.M., Li, A., and Bassik, M.C. (2016). Systematic comparison of CRISPR/Cas9 and RNAi screens for essential genes. *Nat. Biotechnol.* 34, 634–636.
- Morgens, D.W., Wainberg, M., Boyle, E.A., Ursu, O., Araya, C.L., Tsui, C.K., Haney, M.S., Hess, G.T., Han, K., Jeng, E.E., et al. (2017). Genome-scale measurement of off-target activity using Cas9 toxicity in high-throughput screens. *Nat. Commun.* 8, 15178.
- Obeng, E.A., Stewart, C., and Abdel-Wahab, O. (2019). Altered RNA Processing in Cancer Pathogenesis and Therapy. *Cancer Discov.* 9, 1493–1510.
- Oppenheimer, L., Wellner, V.P., Griffith, O.W., and Meister, A. (1979). Glutathione synthetase. Purification from rat kidney and mapping of the substrate binding sites. *J. Biol. Chem.* 254, 5184–5190.
- Park, J.W., Tokheim, C., Shen, S., and Xing, Y. (2013). Identifying differential alternative splicing events from RNA sequencing data using RNASeq-MATS. *Methods Mol. Biol.* 1038, 171–179.
- Pereira, B., Chin, S.F., Rueda, O.M., Volland, H.K., Provenzano, E., Bardwell, H.A., Pugh, M., Jones, L., Russell, R., Sammut, S.J., et al. (2016). The somatic mutation profiles of 2,433 breast cancers refines their genomic and transcriptomic landscapes. *Nat. Commun.* 7, 11479.
- Perry, M.E., Mendrysa, S.M., Saucedo, L.J., Tannous, P., and Holubar, M. (2000). p76(MDM2) inhibits the ability of p90(MDM2) to destabilize p53. *J. Biol. Chem.* 275, 5733–5738.
- Rogers, Z.N., McFarland, C.D., Winters, I.P., Naranjo, S., Chuang, C.H., Petrov, D., and Winslow, M.M. (2017). A quantitative and multiplexed approach to uncover the fitness landscape of tumor suppression *in vivo*. *Nat. Methods* 14, 737–742.
- Sakamuro, D., Elliott, K.J., Wechsler-Reya, R., and Prendergast, G.C. (1996). BIN1 is a novel MYC-interacting protein with features of a tumour suppressor. *Nat. Genet.* 14, 69–77.
- Scheffler, B., Walton, N.M., Lin, D.D., Goetz, A.K., Enikolopov, G., Roper, S.N., and Steindler, D.A. (2005). Phenotypic and functional characterization of adult brain neurogenesis. *Proc. Natl. Acad. Sci. USA* 102, 9353–9358.
- Schröder, M.S., Culhane, A.C., Quackenbush, J., and Haibe-Kains, B. (2011). survcomp: an R/Bioconductor package for performance assessment and comparison of survival models. *Bioinformatics* 27, 3206–3208.

- Schwenk, F., Baron, U., and Rajewsky, K. (1995). A cre-transgenic mouse strain for the ubiquitous deletion of loxP-flanked gene segments including deletion in germ cells. *Nucleic Acids Res.* **23**, 5080–5081.
- Sibley, C.R., Blazquez, L., and Ule, J. (2016). Lessons from non-canonical splicing. *Nat. Rev. Genet.* **17**, 407–421.
- Toledo, F., and Wahl, G.M. (2006). Regulating the p53 pathway: in vitro hypotheses, in vivo veritas. *Nat. Rev. Cancer* **6**, 909–923.
- Tonelli, C., Morelli, M.J., Bianchi, S., Rotta, L., Capra, T., Sabò, A., Campaner, S., and Amati, B. (2015). Genome-wide analysis of p53 transcriptional programs in B cells upon exposure to genotoxic stress in vivo. *Oncotarget* **6**, 24611–24626.
- Tschaharganeh, D.F., Xue, W., Calvisi, D.F., Evert, M., Michurina, T.V., Dow, L.E., Banito, A., Katz, S.F., Kastenhuber, E.R., Weissmueller, S., et al. (2014). p53-dependent Nestin regulation links tumor suppression to cellular plasticity in liver cancer. *Cell* **158**, 579–592.
- Ule, J., and Blencowe, B.J. (2019). Alternative Splicing Regulatory Networks: Functions, Mechanisms, and Evolution. *Mol. Cell* **76**, 329–345.
- Valente, L.J., Gray, D.H., Michalak, E.M., Pinon-Hofbauer, J., Egle, A., Scott, C.L., Janic, A., and Strasser, A. (2013). p53 efficiently suppresses tumor development in the complete absence of its cell-cycle inhibitory and proapoptotic effectors p21, Puma, and Noxa. *Cell Rep.* **3**, 1339–1345.
- Van Nostrand, E.L., Pratt, G.A., Shishkin, A.A., Gelboin-Burkhart, C., Fang, M.Y., Sundaraman, B., Blue, S.M., Nguyen, T.B., Surka, C., Elkins, K., et al. (2016). Robust transcriptome-wide discovery of RNA-binding protein binding sites with enhanced CLIP (eCLIP). *Nat. Methods* **13**, 508–514.
- Van Nostrand, E.L., Pratt, G.A., Yee, B.A., Wheeler, E.C., Blue, S.M., Mueller, J., Park, S.S., Garcia, K.E., Gelboin-Burkhart, C., Nguyen, T.B., et al. (2019). Principles of RNA processing from analysis of enhanced CLIP maps for 150 RNA binding proteins. *Genome Biol.* **21**, 90.
- Varmeh-Ziae, S., Okan, I., Wang, Y., Magnusson, K.P., Warthoe, P., Strauss, M., and Wiman, K.G. (1997). Wig-1, a new p53-induced gene encoding a zinc finger protein. *Oncogene* **15**, 2699–2704.
- Vilborg, A., Glahder, J.A., Wilhelm, M.T., Bersani, C., Corcoran, M., Mahmoudi, S., Rosenstierne, M., Grandér, D., Farnebo, M., Norrild, B., and Wiman, K.G. (2009). The p53 target Wig-1 regulates p53 mRNA stability through an AU-rich element. *Proc. Natl. Acad. Sci. USA* **106**, 15756–15761.
- Vousden, K.H., and Prives, C. (2009). Blinded by the Light: The Growing Complexity of p53. *Cell* **137**, 413–431.
- Wang, L., Brooks, A.N., Fan, J., Wan, Y., Gambe, R., Li, S., Hergert, S., Yin, S., Freeman, S.S., Levin, J.Z., et al. (2016). Transcriptomic Characterization of SF3B1 Mutation Reveals Its Pleiotropic Effects in Chronic Lymphocytic Leukemia. *Cancer Cell* **30**, 750–763.
- Wang, Y., Ji, T., Nelson, A.D., Glanowska, K., Murphy, G.G., Jenkins, P.M., and Parent, J.M. (2018). Critical roles of α II spectrin in brain development and epileptic encephalopathy. *J. Clin. Invest.* **128**, 760–773.
- Wilhelm, M.T., Méndez-Vidal, C., and Wiman, K.G. (2002). Identification of functional p53-binding motifs in the mouse wig-1 promoter. *FEBS Lett.* **524**, 69–72.
- Yoshimura, S., Gerondopoulos, A., Linford, A., Rigden, D.J., and Barr, F.A. (2010). Family-wide characterization of the DENN domain Rab GDP-GTP exchange factors. *J. Cell Biol.* **191**, 367–381.
- Younger, S.T., Kenzelmann-Broz, D., Jung, H., Attardi, L.D., and Rinn, J.L. (2015). Integrative genomic analysis reveals widespread enhancer regulation by p53 in response to DNA damage. *Nucleic Acids Res.* **43**, 4447–4462.
- Zhang, J., and Manley, J.L. (2013). Misregulation of pre-mRNA alternative splicing in cancer. *Cancer Discov.* **3**, 1228–1237.
- Zhang, J., Lieu, Y.K., Ali, A.M., Penson, A., Reggio, K.S., Rabadian, R., Raza, A., Mukherjee, S., and Manley, J.L. (2015). Disease-associated mutation in SRSF2 misregulates splicing by altering RNA-binding affinities. *Proc. Natl. Acad. Sci. USA* **112**, E4726–E4734.

STAR★METHODS

KEY RESOURCES TABLE

REAGENT or RESOURCE	SOURCE	IDENTIFIER
Antibodies		
p53 antibody (CM5)	Leica (Novocastra)	NCL-L-p53-CM5p; RRID: AB_563933
Zmat3/Wig1 antibody	Santa Cruz	sc-398712
Zmat3 antibody	Proteintech	10504-1-AP; RRID: AB_2217579
Ptpn14/Pez (F-12) antibody	Santa Cruz	sc-373766; RRID: AB_10917236
BrdU antibody	Becton Dickinson	555627; RRID: AB_10015222
Mdm4 antibody	Sigma-Aldrich	M0445; RRID: AB_532256
HA antibody	Cell Signaling Technologies	#3724; RRID: AB_1549585
Ki67 antibody	BD Biosciences	550609; RRID: AB_393778
Cleaved Caspase 3 antibody	Cell Signaling Technologies	#9664; RRID: AB_2070042
Goat-anti-rabbit HRP antibody	Jackson ImmunoResearch	11-035-144; RRID: AB_11035144
Goat-anti-mouse HRP antibody	Jackson ImmunoResearch	115-035-146; RRID: AB_2307392
Goat biotinylated anti-rabbit IgG	Vector Labs	BA-1000; RRID: AB_2313606
Horse biotinylated anti-mouse IgG	Vector Labs	BA-2000; RRID: AB_2313581
Anti-mouse Alexa Fluor 546-labeled secondary antibody	Vector Labs	A11003; RRID: AB_141370
Anti-rabbit fluorescein-labeled secondary antibody	Vector Labs	Fl-1000; RRID: AB_2336197
Gapdh antibody	Fitzgerald	10R-G109A; RRID: AB_1285808
Alpha-Tubulin antibody	Sigma-Aldrich	T6074; RRID: AB_477582
Bacterial and Virus Strains		
Ad-Cre or Ad5CMVCre	University of Iowa	VVC-U of Iowa-5
Ad-empty or Ad5CMVempty	University of Iowa	VVC-U of Iowa-272
Chemicals, Peptides, and Recombinant Proteins		
5-Bromo-2'-deoxyuridine (BrdU)	Millipore Sigma	203806
Lipofectamine 2000	Thermo Fisher	11668019
Critical Commercial Assays		
TruSeq RNA Library Prep Kit (v.2)	Illumina	RS-122-2001
POWER SYBR Green PCR Master Mix	Thermo Fisher	4367660
TRIzol reagent	Thermo Fisher	15596026
M-MLV Reverse Transcriptase	Thermo Fisher	28025013
DAB Peroxidase (HRP) Substrate Kit (with Nickel), 3,3'-diaminobenzidine	Vector Laboratories	SK-4100
VECTASTAIN Elite ABC HRP Kit (Peroxidase, Standard)	Vector Laboratories	PK-6100
ECL prime Western Blotting System	Millipore Sigma	GERPN2232
Deposited Data		
Mendeley Data	This paper	https://dx.doi.org/10.17632/6bkjdg5g85.1
Hras ^{V12} -expressing MEFs homozygous for different <i>Trp53</i> alleles	Brady et al., 2011	GEO: GSE27901
Mouse p53 ChIP-seq	Kenzelmann Broz et al., 2013	GEO: GSE46240
Human p53 ChIP-seq	Younger et al., 2015	GEO: GSE55727
TCGA human cancer data	Genomic Data Commons	https://gdc.cancer.gov
METABRIC human breast cancer data	European Genome-Phenome Archive	https://ega-archive.org/dacs/EGAC00001000484

(Continued on next page)

Continued

REAGENT or RESOURCE	SOURCE	IDENTIFIER
Achilles DepMap (CCLE_Depmap_18q3 release)	Meyers et al., 2017	https://depmap.org/portal/download/
Zmat3 RNA-seq	This paper	GEO: GSE145430
Zmat3 eCLIP	This paper	GEO: GSE14555
Experimental Models: Cell Lines		
Mouse: p53 ^{WT} MEFs	Laboratory of Laura Attardi	N/A
Mouse: H11 ^{Cas9/Cas9} ; p53 ^{WT/WT} MEFs	Laboratory of Laura Attardi	N/A
Mouse: p53 ^{-/-} MEFs	Laboratory of Laura Attardi	N/A
Mouse: Zmat3 ^{-/-} MEFs	Laboratory of Andreas Strasser	N/A
Mouse: p53 ^{WT} non-small cell lung cancer cell line: <i>Kras</i> ^{LA2/+} ; <i>Trp53</i> ^{LSL-WT/LSL-WT}	Laboratory of Laura Attardi	N/A
Mouse: Eμ-Myc B cell lymphoma cells: <i>Eμ-myc; Trp53</i> ^{ER/-}	Laboratory of Lin He	N/A
Human: H23 lung adenocarcinoma	ATCC	CRL-5800
Human: Fibroblasts	Coriell Cell Repositories	GM00011, GM06170
Experimental Models: Organisms/Strains		
Mouse: ICR-Scid: IcrTac:ICR- <i>Prkdc</i> ^{Scid}	Taconic	ICRSC-M
Mouse: <i>Kras</i> ^{LSL-G12D} mice: B6.129S4-Kras ^{tm4Tyj}	Laboratory of Tyler Jacks	N/A
Mouse: <i>Trp53</i> ^{fl/fl} mice: B6.129P2-Trp53 ^{tm1Bm/J}	The Jackson Laboratory	008462
Mouse: Rosa26 ^{LSL-tdTomato}	Madisen et al., 2010	N/A
Mouse: H11 ^{LSL-Cas9} . B6.129- <i>Igs2</i> ^{tm1(CAG-cas9+)Mmw} /J	Chiou et al., 2015; The Jackson Laboratory	026816
Mouse: CMV-Cre: B6.C-Tg(CMV-cre) 1Cgn/J	Schwenk et al., 1995; The Jackson Laboratory	006054
Mouse: C57BL/6	Charles River Laboratories	C57BL/6NCrl
Oligonucleotides		
See Table S7 for primers	This paper	N/A
Recombinant DNA		
Lentiviral shRNA TSAG library	This manuscript	N/A
Lentiviral sgRNA TSAG library- Pool 1	This manuscript	N/A
Lentiviral sgRNA TSAG library- Pool 2	This manuscript	N/A
Lentiviral sgRNA mouse safe harbor library (250)	Laboratory of Michael Bassik	N/A
pMCB246 shRNA vector with shRNAs targeting Luciferase, <i>Trp53</i> , <i>Zmat3</i> , <i>Ptpn14</i> , <i>Trp53inp1</i>	Laboratory of Michael Bassik; this manuscript	N/A
pMCB320 sgRNA vector with sgRNAs targeting <i>p53</i> , <i>Zmat3</i> , <i>Dennd2c</i> , <i>Zmat3 RE</i> , or safe harbor controls	Han et al., 2017; this manuscript	Addgene: 89359
pGH020 sgRNA vector with sgRNAs targeting <i>Zmat3</i> , <i>Dennd2c</i> , or safe harbor controls	Hess et al., 2016; this manuscript	Addgene: 85405
Lenti-pLL3.3: sgNT1/Cre	Laboratory of Monte Winslow	Addgene: 66895
Lenti-pLL3.3: sgNT3/Cre	Laboratory of Monte Winslow	Addgene: 89654
Lenti-pLL3.3 sgp53	This manuscript	N/A
Lenti-pLL3.3 sgZmat3 (1-3)	This manuscript	N/A
pT3-Caggs-Kras G12D-IRES-EGFP	This manuscript	N/A

(Continued on next page)

Continued

REAGENT or RESOURCE	SOURCE	IDENTIFIER
CMV-SB13 transposase	Huang et al., 2014	N/A
px330-U6-sgRNA-CMV-spCas9	Cong et al., 2013	Addgene: 42230
pcDNA3.1-3XHA-GFP	Brady et al., 2011	N/A
pcDNA3.1-3XHA-p53	Brady et al., 2011	N/A
pcDNA3.1-3XHA-Zmat3	This manuscript	N/A
pcDNA3.1-3XHA-Zmat3R99Q	This manuscript	N/A
Software and Algorithms		
Enrichr	Kuleshov et al., 2016	https://maayanlab.cloud/Enrichr/
Survcomp	Schröder et al., 2011	http://bioconductor.org/packages/release/bioc/html/survcomp.html
Galaxy	Afgan et al., 2018	https://usegalaxy.org/
DEseq2	Love et al., 2014	https://bioconductor.org/packages/release/bioc/html/DESeq2.html
DISCOVER package	Canisius et al., 2016	https://ccb.nki.nl/software/discover/
Maftools	Mayakonda and Koeffler, 2016	https://www.bioconductor.org/packages/release/bioc/html/maftools.html
CasTLE	Morgens et al., 2016	https://bitbucket.org/dmorgens/castle
Cutadapt (1.14.0)	Martin, 2011	https://code.google.com/p/cutadapt/
STAR (2.4.0i)	Dobin et al., 2013	https://github.com/alexdobin/STAR/releases/tag/STAR_2.4.0i
makebigwigfiles	Laboratory of Gene Yeo	https://github.com/yeolab/makebigwigfiles
rMATS (3.2.5)	Park et al., 2013	http://rnaseq-mats.sourceforge.net/
Featurecounts (1.5.3)	Liao et al., 2014	http://bioinf.wehi.edu.au/subread-package/
ImageJ	NIH	https://imagej.nih.gov
ICE v2 CRISPR analysis	Synthego	https://www.synthego.com/products/bioinformatics/crispr-analysis

RESOURCE AVAILABILITY**Lead Contact**

Further information and requests for resources and reagents should be directed to the Lead Contact, Laura D. Attardi (attardi@stanford.edu).

Materials Availability

Plasmids generated by this study are available upon request.

Data and Code Availability

The microarray data were published previously (Brady et al., 2011) and are available in the Gene Expression Omnibus (GEO: GSE27901). The mouse and human ChIP-seq data were also published previously (Kenzelmann Broz et al., 2013; Younger et al., 2015) and are available in the Gene Expression Omnibus (GEO: GSE46240, GSE55727). The human cancer data that support the findings of this study are available from the Genomic Data Commons, <https://gdc.cancer.gov>, and the European Genome-Phenome Archive, <https://ega-archive.org/dacs/EGAC00001000484>. The Achilles DepMap dataset (DepMap: CCLE_Depmap_18q3 release) is available from the DepMap portal, <https://depmap.org/portal/download/>. The Zmat3 RNA-seq (GEO: GSE145430) and eCLIP data (GEO: GSE14555) have been submitted to the Gene Expression Omnibus. Scripts for version 1.0 of casTLE (Morgens et al., 2016) are available at <https://bitbucket.org/dmorgens/castle>. Original data have been deposited to Mendeley Data: <https://dx.doi.org/10.17632/6bkjd5g85.1>.

EXPERIMENTAL MODEL AND SUBJECT DETAILS**Subcutaneous tumor model**

All animal experiments were in accordance with the Stanford University APLAC (Administrative Panel on Laboratory Animal Care). Cells were suspended in PBS at 3 million cells per 100 µL (library experiments) or 1 million cells per 100 µL (*in vivo* competition experiments). For the library experiments, cells were mixed 1:1 in Matrigel® (Corning). 100 µL (*in vivo* competition experiments) or 200 µL (library experiments) of cell suspension were injected under the skin on the right and left flanks of 6-week-old male ICR/Scid mice (Taconic). Tumors were harvested after three weeks of growth. For library experiments, frozen tumors were ground in liquid nitrogen, followed by genomic DNA preparation (Gentra Puregene). ICR/Scid mice were group-housed (up to 5 mice per cage), and irradiated chow and water were provided *ad libitum*.

Mouse lung adenocarcinoma study

All animal experiments were in accordance with the Stanford University APLAC (Administrative Panel on Laboratory Animal Care). Mice were group-housed (up to 5 mice per cage), and food and water were provided *ad libitum*. *Kras*^{LSL-G12D/+}; *Rosa26*^{LSL-tdTomato/LSL-tdTomato}; *H11*^{LSL-Cas9/LSL-Cas9} (*KT;H11*^{LSL-Cas9}) and *Kras*^{LSL-G12D/+;p53}^{flox/flox}; *Rosa26*^{LSL-tdTomato/LSL-tdTomato}; *H11*^{LSL-Cas9/LSL-Cas9} (*KPT;H11*^{LSL-Cas9}) mice have been described (Chiou et al., 2015; Jackson et al., 2001; Madisen et al., 2010). Three unique sgRNAs targeting Zmat3 (selected from those used in the screen, sgZmat3.1: CTCCCCCTGCCGTGGCAC, sgZmat3.2: CCACCAACGCTGCTCACCC, sgZmat3.3: GGCTTACACAGCTCCTCCA), one previously characterized p53 sgRNA (AGGAGGCTCCT GACACTCGGA), and two previously characterized negative control sgRNAs (sgNT.1: GCGAGGGTATTGGCTCCGCG, sgNT.2: CCGCGCCGTTAGGGAACGAG) were used for these experiments (Rogers et al., 2017). Lenti-sgRNA/Cre vectors were generated using standard methods (Chiou et al., 2015). Lung tumors were induced as previously described (DuPage et al., 2009). Specifically, 6–12 week old male and female *KT;H11*^{LSL-Cas9} or *KPT;H11*^{LSL-Cas9} mice were randomly assigned to experimental groups, and then anesthetized by intraperitoneal injection of Avertin (2-2-2 Tribromoethanol). 90,000 particles of Lenti-U6-sgRNA/PGK-Cre virus were suspended in 50 µL sterile PBS and delivered intratracheally. Lungs were harvested 17–20 weeks after infection and fixed in formalin for 24 h before processing and H&E staining.

Mouse HCC study

The Memorial Sloan Kettering Cancer Center (MSKCC) Animal Care and Use Committee (protocol no. 11-06-011) approved all mouse experiments. Mice were maintained under specific pathogen-free conditions, and food and water were provided *ad libitum*. Liver tumorigenesis was induced by delivery of plasmids via hydrodynamic tail vein injection (Moon et al., 2019). Specifically, a mixture of sterile 0.9% NaCl solution and plasmids containing pT3-Caggs-Kras^{G12D}-IRES-GFP (5 µg), CRISPR plasmid px330 DNA (Cong et al., 2013) expressing Cas9 and a single guide RNA (sgRNA) targeting Chromosome 8 (negative control), p53 or Zmat3 (25 µg), and CMV-SB13 transposase (Huang et al., 2014) (6 µg) was prepared for each injection. sgRNA sequences used for cloning into px330 are as follows: Chromosome 8 oligo (GACATTCTTCCCCACTGG); Trp53 oligo (GACCCTGTCACCGA GACCCC); Zmat3 oligo 1 (AGAGGATTTAGCTAAGAGAG); Zmat3 oligo 2 (GCCAGGGGGCAGGGTGATCC). Female C57BL/6 mice (6–8 weeks of age) from Charles River Laboratories were randomly assigned to experimental groups to be injected with the 0.9% NaCl solution/plasmid mix into the lateral tail vein, with a total volume corresponding to 10% of body weight in 5 to 7 s. Upon sacrifice, numbers and diameters of macroscopic liver tumors were recorded, and liver tissues were excised and fixed in formalin for 24 h before processing and H&E staining.

Mouse cell culture and viral infections

MEFs were derived from E13.5 embryos (Brady et al., 2011). *H11*^{Cas9/+} MEFs were generated by crossing *H11*^{LSL-Cas9/LSL-Cas9} mice to CMV-Cre mice (Schwenk et al., 1995). To generate *E1A;Hras*^{G12V}; *p53*^{+/+} or *E1A;Hras*^{G12V}; *p53*^{+/+}; *Cas9* MEFs, wild-type or *H11*^{Cas9/+} MEFs were transduced with *E1A* and *Hras*^{GV12}-expressing retroviruses (Brady et al., 2011). For library experiments, virus was produced in 15 cm plates, and target cells in 15 cm plates were transduced at a MOI of ~0.2, as measured by expression of the mCherry marker. Cells were selected in puromycin (2 µg/mL) for ~10 days prior to collection of time zero samples or injection into mice. Lung adenocarcinoma cell lines were generated from lung tumors dissected from 11-week-old *Kras*^{LA2/+}; *Trp53*^{LSL-wt/LSL-wt} mice. *Kras*^{LA2/+}; *Trp53*^{LSL-wt/LSL-wt} mice spontaneously recombine to express an oncogenic *Kras*^{G12D} allele (Johnson et al., 2001). Cultures were established in N5 medium (Scheffler et al., 2005) supplemented with EGF (20 ng/mL) and FGF (20 ng/mL), then sorted by fluorescence-activated cell sorting (FACS) (Stanford Shared FACS facility) for EpCam positivity (BioLegend), and later switched to DMEM high-glucose media supplemented with 10% FBS. For Adenovirus infections, cells were seeded at 1 × 10⁵ cells/well in 6-well plates, then infected with either Ad5CMVempty (Ad-Empty, Cat# VVC-U of Iowa-272) or Ad5CMVCre (Ad-Cre, Cat# VVC-U of Iowa-5), obtained from the University of Iowa Viral Vector Core, at an MOI of 100. Cells were harvested for RNA preparation 48 h after infection. *Eμ-Myc* lymphoma cells expressing a tamoxifen-inducible *p53*-Estrogen receptor fusion protein (Christophorou et al., 2005) (*p53*^{-ER-TAM}) were the kind gift of Lin He. Cells were grown on a feeder layer (irradiated 3T3 cells) and treated with 1 µM 4-hydroxytamoxifen (4OHT) or Ethanol (vehicle) and harvested for RNA preparation after 6 h. Unless otherwise indicated, all cells were maintained in DMEM high-glucose media (GIBCO) supplemented with 10% FBS at 37°C and 5%CO₂.

The sex of the mouse cell lines was not determined as it was not expected to impact the results. Cell line authentication was not applicable.

Human cell culture

Human fibroblasts were obtained from Coriell Cell Repositories (GM00011, GM06170) and maintained in DMEM high-glucose media supplemented with 15% FBS at 37°C and 5%CO₂. H23 human lung adenocarcinoma cells were maintained in DMEM high-glucose media supplemented with 10% FBS at 37°C and 5%CO₂. All human cell lines are male and were not authenticated.

METHOD DETAILS

TSAG identification

Using microarray data from mouse embryonic fibroblasts (MEFs) expressing oncogenic *Hras*^{G12V} (Brady et al., 2011), we compared the expression profiles of cells expressing p53 TAD mutants active in tumor suppression (wild-type p53, p53^{53,54}, and p53^{25,26}) with expression profiles of cells expressing p53 mutants inactive in tumor suppression (p53^{25,26,53,54} and p53 null), and identified genes induced at least 2-fold in the active group, yielding a list of 55 activated genes. We also identified a list of 58 genes induced 2-fold or greater in *Hras*^{G12V} p53^{25,26}-expressing MEFs relative to *Hras*^{G12V} p53 null MEFs and at least 70% as well as by wild-type p53 relative to p53 null cells. These combined lists comprise 87 TSAGs. To determine whether the TSAGs are direct p53 targets, they were analyzed for p53-bound response elements (RE) near or within their gene body using ChIP-seq datasets from mouse embryonic fibroblasts, stem cells, or splenocytes (Brady et al., 2011; Kenzelmann Broz et al., 2013; Lee et al., 2010; Li et al., 2012a; Tonelli et al., 2015) (Table S1).

Library design, amplification, and sequencing

25 shRNAs targeting each TSAG were drawn from a previously validated shRNA library (Kampmann et al., 2015), along with 1000 non-targeting shRNAs, and used as single library. 10 sgRNAs targeting each TSAG were drawn from a previously designed mouse-targeting library (Morgens et al., 2017); the guides were split into two pools along with 250 negative control safe-harbor sgRNAs each, which target predicted non-functional regions in the mouse genome to replicate the effects of DNA damage (Morgens et al., 2017). This resulted in two separate sgRNA libraries, each targeting a different set of genes but containing the same negative controls. shRNA and sgRNA libraries were synthesized and cloned (Kampmann et al., 2015; Morgens et al., 2017). The composition of the shRNA and sgRNA libraries were monitored by amplicon sequencing on a MiSeq (for shRNA libraries) and on a NextSeq (for sgRNA libraries) (Deans et al., 2016).

Analysis of shRNA library screens

Due to the size of the shRNA library, we relied on the observation of multiple, independent shRNAs highly represented relative to negative control shRNAs in a given tumor. The 22 base pairs of each shRNA were aligned to a library index using Bowtie (Langmead et al., 2009) with zero mismatches allowed. shRNAs were then tested for enrichment over the negative controls in each individual tumor. First, shRNAs with zero or one count were removed. Then, shRNAs with a greater number of counts than at least 95% of the remaining non-targeting controls detected were considered enriched in that tumor. This analysis was repeated for each tumor, and for each gene, the number of shRNAs targeting that gene that were enriched in at least one tumor were counted. Note that shRNAs that were enriched in multiple tumors were not counted multiple times. This number of enriched shRNAs targeting each gene was then compared to the total number of shRNAs targeting that gene detected. In order to calculate significance, a similar analysis was performed with the non-targeting controls, where the top 5% of non-targeting controls from each tumor were counted (again not counting the same control shRNA multiple times) and compared to the total number of non-targeting controls detected across all tumors. The number of enriched shRNAs targeting each gene was then compared to the fraction of enriched non-targeting controls using a hypergeometric test (i.e., sampling without replacement) to calculate a p value.

Analysis of CRISPR-Cas9 library screens

The first 17 base pairs of the reads were aligned to the sgRNA library using Bowtie (Langmead et al., 2009) with zero mismatches allowed. Enrichment of each element was then calculated as a log base 2 ratio of the fraction of the counts in the tumor versus the time zero sample. Gene level data were then calculated with the safe-targeting guides as negative controls using version 1.0 of casTLE (Morgens et al., 2016). To identify consistent results across all 6 biological replicates for each library, the estimated casTLE effects for each gene from all 6 tumors were compared to a background of estimated casTLE effects of all genes from all 6 tumors. A Mann-Whitney U test was then used to calculate p values.

Transformation assays

Anchorage-independent growth assays were performed by plating 3,000 cells per well in triplicate in 6-well plates. Cells were plated in phenol red-free DMEM containing 10% FBS, 50 U/mL penicillin/streptomycin and 0.3% agarose, on a layer of media containing DMEM with 10% FBS, 50 U/mL penicillin/streptomycin and 0.5% agarose, and grown for three weeks. After three weeks, cells were stained using a Giemsa solution (0.02% in PBS) and scored using ImageJ software.

In vivo competition assay

E1A;Hras^{G12V};p53^{+/+};Cas9 MEFs were transduced with lentiviruses expressing *Zmat3*, *Dennd2c*, or negative control sgRNAs along with GFP (Hess et al., 2016) or mCherry (Han et al., 2017) fluorescent markers. Cells with sg*Zmat3* or sg*Dennd2c* and GFP or mCherry were mixed 1:1 with cells expressing a negative control sgRNA and the opposite marker. This input mixture of cells was analyzed for the GFP to mCherry ratio by flow cytometry (LSR Fortessa, BD Biosciences). Cells were then injected into mice and grown as subcutaneous tumors as described above. After three weeks, tumors were harvested and incubated in RPMI media with Liberase (20 µg/mL, Roche) and DNase (400 µg/mL, Roche) enzymes, then filtered, centrifuged with 30% Percoll (Sigma), washed in RPMI and analyzed for GFP and mCherry expression by flow cytometry (LSR Fortessa, BD Biosciences).

Analysis of CRISPR indels

Genomic DNA was extracted from *E1A;Hras^{G12V};Cas9* MEFs expressing sgRNAs using the DNeasy Blood and Tissue kit (QIAGEN). The intended sgRNA target sites were PCR amplified using primers designed to flank the site. PCR products were separated on agarose gels and the amplified products extracted using a Gel Extraction Kit (QIAGEN). The DNA fragments were Sanger sequenced by Quintara Biosciences (Berkeley, CA). Sequencing files were submitted to ICE v2 CRISPR analysis tool (Synthego, Menlo Park, CA).

qRT-PCR and Semiquantitative PCR

Trizol reagent (Invitrogen) was used for RNA preparation, and reverse transcription was performed with MMLV reverse transcriptase (Invitrogen). Quantitative PCR was performed in triplicate using gene-specific primers and SYBR green (Life Technologies) in a 7900HT Fast Real-Time PCR machine (Applied Biosystems). Changes in transcript abundance were calculated using the standard curve method. Semiquantitative PCR was performed for 27, 32, or 35 cycles (45 s 95°C; 30 s at 58°C; 40 s at 72°C) using a ~34-ng cDNA template. Products were visualized on a 2% agarose gel. Primer sequences are in Table S7.

ChIP

E1A;Hras^{G12V};Cas9 MEFs were seeded at 7.5×10^6 cells per 10-cm dish and ChIP was performed the following day. Briefly, cells were crosslinked at room temperature by treatment with DMEM media with 1% formaldehyde, and the reaction was quenched by addition of glycine to a final concentration of 0.125 M. After washing with cold 1X PBS, cells were harvested by scraping in lysis buffer (5 mM PIPES pH 8.0, 85 mM KCl, 0.5% NP-40) and pelleted. Cell pellets were processed by passage through a 21-gauge needle 20 times. Lysates were pelleted and resuspended in RIPA buffer. Sonication was performed in a Bioruptor sonicator (Diagenode) to shear chromatin to a size range of ~200–700 bp. Anti-p53 antibody (CM5, Leica Novocastra) was coupled to ChIP-grade protein A/G magnetic beads (Thermo Scientific) overnight. After saving 10% for an input sample, samples were immunoprecipitated for one h at room temperature and one h at 4°C, and washes were performed two times with low-salt wash buffer (0.1% SDS, 1% Triton X-100, 2 mM EDTA, 20 mM Tris-HCl at pH 8.1, 150 mM NaCl), three times with high-salt wash buffer (0.1% SDS, 1% Triton X-100, 2 mM EDTA, 20 mM Tris-HCl at pH 8.1, 500 mM NaCl), and four times with LiCl wash buffer (0.25 M LiCl, 1% IGEPAL CA630, 1% deoxycholic acid sodium salt, 1 mM EDTA, 10 mM Tris at pH 8.1). Input was reverse crosslinked by treatment with ProK, RNase A, and incubation at 65°C. All samples were purified by PCR Purification Kit (QIAGEN). Chromatin-immunoprecipitated DNA was quantified by qPCR using SYBR Green (SA-Biosciences) and a 7900HT Fast Real-Time PCR machine (Applied Biosystems).

Western blots

Western blots were performed according to standard protocols. Briefly, cells were lysed in RIPA buffer, extracts were run on SDS-PAGE gels, gels were transferred to PVDF membrane (Immobilon, Millipore), and membranes were blocked with 5% milk and probed with antibodies directed against *Zmat3* (1:100, Santa Cruz), p53 (CM5, 1:500 Leica Novocastra), *Ptpn14* (1:100, Santa Cruz), or *Gapdh* (1:15,000, Fitzgerald), followed by anti-mouse or anti-rabbit HRP-conjugated secondary antibodies (Vector Laboratories). Blots were developed with ECL Prime (Amersham) and imaged using a ChemiDoc XRS+ (BioRad).

Immunohistochemistry

Hematoxylin and eosin (H&E) staining and immunohistochemistry were performed on paraffin-embedded lungs using standard protocols. Immunohistochemistry was performed using antibodies directed against Ki67 (1:100, BD Biosciences,) and Cleaved caspase 3 (1:400, Cell Signaling Technologies). Briefly, paraffin sections were re-hydrated, unmasked in 10mM Sodium Citrate buffer with 0.05% Tween 20 in a pressure cooker for 10 min, the peroxidase was quenched for 15 min in 3% H₂O₂, sections were blocked for 30 min in TBS with 0.025% Triton X-100 supplemented with 10% serum and 1% BSA, and incubated overnight at 4°C with primary antibody. On the next day, the sections were incubated for 30 min with biotinylated antibody compatible with the primary antibody used (1:1000, Vector Laboratories) and were subsequently incubated with VECTASTAIN Elite ABC HRP Kit (Vector Laboratories), according to manufacturer's instructions. The sections were washed with TBS in between steps. Staining was performed using the DAB peroxidase kit (Vector Laboratories) and hematoxylin (H-3401, Vector Laboratories) for counter-staining. A Leica DM6000B microscope (Leica Microsystems) or NanoZoomer 2.0-RS slide scanner (Hamamatsu) was used for imaging.

Overexpression and immunofluorescence

Overexpression experiments for BrdU incorporation analysis were performed using constructs in which Zmat3 cDNA was cloned into a pcDNA vector carrying an HA-tag. The pcDNA3.1-3XHA-Zmat3 construct was generated by PCR amplification and insertion of the cDNA into Ascl and Pael restriction sites in pcDNA3.1-3XHA plasmid (gift of S. Artandi). The pcDNA3.1-3XHA-p53 and pcDNA3.1-3XHA-GFP constructs have been described (Brady et al., 2011). The pcDNA3.1-3XHA-Zmat3 plasmid was used as a template for site-directed mutagenesis to generate pcDNA3.1-3XHA-Zmat3R99Q. KOD Xtreme Hot Start DNA Polymerase (71975-M, Sigma-Aldrich) was used to amplify the template with a pair of primers (forward primer 5'-catggcaagaaactacaaaattattaccgacgt-3'; and reverse primer: 5'-agctgcgtataattttagtttcttgccatg -3'), and the mutation was verified by Sanger sequencing. p53 null MEFs and H23 cells were transfected with the constructs using Lipofectamine 2000 (Invitrogen), according to manufacturer instructions. Twenty-four h later, cells were pulsed with 3 µg/mL BrdU for 4 h, fixed in 4% paraformaldehyde for 15 min, washed in PBS, permeabilized in PBS + 0.25% Triton X-100 for 15 min, washed in PBS, incubated with anti-HA (1:400, Cell Signaling Technologies) antibody overnight at 4°C, washed in PBS, and subsequently incubated with anti-rabbit fluorescein-labeled secondary antibody (1:200, Vector Laboratories) for 1 h. The cells were then post fixed with 4% paraformaldehyde, washed and treated with hydrochloric acid (1.5 N) for DNA denaturation. Next, the cells were washed in PBS, incubated with anti-BrdU antibody (1:50, BD PharMingen), washed in PBS, and incubated with anti-mouse Alexafluor 546-labeled secondary antibody (1:200, Invitrogen). Images were taken using a Leica DM6000B microscope (Leica Microsystems).

Human cancer data analysis

Expression of ZMAT3 was evaluated in human tumors with wild-type or mutant TP53 using TCGA data available via the Genomic Data Portal (<https://gdc.cancer.gov>) and the METABRIC breast cancer dataset (Curtis et al., 2012; Pereira et al., 2016) (<https://www.ebi.ac.uk/ega/studies/EGAS00000000083>). ZMAT3 expression was adjusted by copy number status to control for the effect of amplifications caused by the proximity of ZMAT3 to PIK3CA, a known driver of tumorigenesis, to ensure that we examined the effect of ZMAT3 expression and not PI3KCA amplification. Samples were stratified based on TP53 status. Confidence intervals were calculated at 95%. Clinical outcome analyses were generated based on disease-specific survival for the METABRIC breast cancer dataset. A log rank test measuring the difference in survival between samples with high expression (1st tertile) and low expression (3rd tertile) of ZMAT3 or DENND2C was performed. Additionally, a Cox Proportional Hazard model was built to evaluate the association between expression and outcome while adjusting for age, grade, size, lymph node number and ER and HER2 status in the breast cancer analysis and age, gender and stage in the LIHC and LUAD analyses. Mutual exclusivity between TP53 and ZMAT3 or DENND2C mutations was evaluated in uterine (UCEC) cancer using data from TCGA. The DISCOVER method, which robustly controls the false positive rate (Canisius et al., 2016), was used to test for mutual exclusivity, and the accompanying p value is reported. For survival analysis, the packages “survival,” “rms” and “survcomp” were used (Schröder et al., 2011). Oncoplot were generated with package “maf-tools” (Mayakonda and Koeffler, 2016).

ZMAT3 eCLIP and data analysis

ZMAT3 eCLIP was performed by Eclipse BioInnovations Inc (San Diego) with slight modifications to the published eCLIP protocol. Polyclonal populations of *E1A;Hras^{G12V};Cas9* MEFs expressing one of three different NC sgRNAs and one *E1A;Hras^{G12V}* Zmat3-knockout MEF sample (Janic et al., 2018) were used for the experiment. Briefly, 20 million cells were UV crosslinked (254nM, 400 mJ/cm²) and lysed in 1 mL of 4°C eCLIP lysis buffer (50 mM TrisHCl pH 7.4, 100 mM NaCl, 1% NP-40, 0.1% SDS, 0.5% sodium deoxycholate, 1:200 Protease Inhibitor Cocktail III [EMD Millipore], 440 U Murine RNase Inhibitor (Vilborg et al.)). The extract was sonicated (Qsonica Q800R2, 15 cycles of 20 s on/40 s off), incubated with 40 U of RNase I (Ambion) and 4 U Turbo DNase (ThermoFisher) for 5 min at 37°C, and clarified by centrifugation (15k g, 15 min at 4°C). Anti-ZMAT3 antibody (10504-1-AP, Proteintech) was pre-coupled to sheep anti-rabbit IgG Dynabeads (ThermoFisher) and added to clarified lysate followed by incubation overnight at 4°C with rotation. 2% of lysate was removed as paired input, and the remainder was washed with eCLIP high- and low-salt wash buffers. Dephosphorylation (FastAP, ThermoFisher and T4 PNK, NEB) treatment and high efficiency ligation of InvRIL19 (/5Phos/rArGrAr-UrCrGrGrArGrArCrArCrCrUrC/3SpC3/) RNA adaptor (T4 RNA Ligase I (NEB)) was performed as previously described. After one additional high salt buffer wash and two additional wash buffer washes, samples were denatured in 1X NuPAGE buffer with 0.1 M DTT. For chemiluminescent imaging, 10% of ZMAT3 IP and 1% of input were run on NuPAGE 4%-12% Bis-Tris protein gels, transferred to PVDF membrane, probed with ZMAT3 antibody (1:1000, sc398712, Santa Cruz) and 1:8,000 EasyBlot anti Mouse IgG (HRP) (GeneTex), and imaged with C300 Imager using Azure Radiance ECL. For RNA extraction, 80% of ZMAT3 IP and 50% of input were run on NuPAGE 4%-12% Bis-Tris protein gels, transferred to nitrocellulose membrane, and the region from 35 to 110 kDa (protein size to 75kDa above) was isolated from the membrane, finely fragmented, and treated with 20 µL Proteinase K (NEB) plus 130 µL PKS buffer (10 mM TrisHCl pH 7.4, 50 mM NaCl, 10 mM EDTA, 0.2% SDS). An additional 55 µL of water was added, and RNA was then purified by RNA Clean & Concentrator column cleanup (Zymo). Reverse transcription was performed with 120 U Superscript III (ThermoFisher) with InvAR17 primer (CAGACGTGTGCTCTCCGA) at 55°C for 20 min, followed by addition of 2.5 µL ExoSAP-IT and incubation at 37°C for 15 min. After addition of 1 µL 0.5M ETDA, RNA was removed by addition of 3 µL 1M NaOH and incubation at 70°C for 10 min. 3 µL of 1M HCl was added to normalize pH, and RNA was purified with MyOne Silane beads (ThermoFisher). Ligation of InvRand3Tr3 adaptor (/5Phos/NNNNNNNNNAGATCGGAAGAGCGTCGTGT/3SpC3/) to the 5' end of cDNA was performed with T4 RNA Ligase plus the addition of 15 U 5' Deadenylose (NEB). After RNA purification with MyOne Silane beads (ThermoFisher), PCR

amplification (Q5 Master Mix, NEB) was performed with standard Illumina multiplexing indexes, and samples were sequenced on the HiSeq4000 platform.

Analysis of eCLIP data was performed as previously described (Van Nostrand et al., 2016), using the UCSC GRCh38/mm10 genome build with GENCODE Release M20 (GRCh38.p6) transcript annotations. For each sample (sgNC1, sgNC2, sgNC3), ZMAT3-bound RNAs were identified by calculating enrichment of sequencing reads in the eCLIP sample relative to the reads in the input and the ZMAT3-deficient sample. Meta-exon maps were generated as previously described (Van Nostrand et al., 2019). Briefly, for each gene in Gencode v19, the transcript with the highest abundance in the three control *E1A;Hras^{G12V};Cas9* sgNC RNA-seq datasets was chosen as the representative transcript, and genes with representative transcript with TPM < 1 were discarded. Next, for all internal exons (excluding the first and last exons), the region from 500nt upstream to 500nt downstream (for introns less than 1000nt, the region was split, with half assigned to the upstream exon and half to the downstream exon) was queried for the presence of significant peaks. Finally, the number of peaks at each position was averaged over all events to obtain the final meta-exon value. To generate confidence intervals, bootstrapping was performed by randomly selecting (with replacement) the same number of transcripts and calculating the average position-level peak coverage as above, with the 5th and 95th percentiles (out of 100 permutations) shown. Human comparison eCLIP meta-exon plots were obtained from published data (Van Nostrand et al., 2019).

RNA-seq

E1A;Hras^{G12V};Cas9 MEFs were transduced with lentiviruses expressing one of three unique *Zmat3* or one of three unique negative control sgRNAs, selected in puromycin for 3 days, and cultured an additional 10 days. RNA was extracted from cultured cells using RNeasy Mini kit (QIAGEN). RNA-seq libraries were prepared using the Illumina TruSeq Kit (v.2), according to the manufacturer's instructions. RNA-seq reads were aligned to the mouse genome (mm10) and analyzed using the public server Galaxy (<https://usegalaxy.org>; Afgan et al., 2018), which employs the STAR aligner (Dobin et al., 2013) and DESeq2 (Love et al., 2014) for differential expression analysis. Significantly differentially expressed transcripts were identified using an adjusted p value cutoff of < 0.05. Enrichr (<https://maayanlab.cloud/Enrichr/>) was used to identify enriched gene ontology (GO) terms (Kuleshov et al., 2016).

RNA-seq alternative splicing analysis

First, fastq files were processed using cutadapt (1.14.0) (Martin, 2011) to trim adapters and low quality sequences. Next, trimmed reads were first aligned using STAR (2.4.0i) (Dobin et al., 2013) against repeat elements (RepBase 18.05) with aligning reads removed from further analysis. Remaining non-repeat reads were then mapped against the mouse assembly (mm10) to generate corresponding bam files. Bigwigs were generated using an in-house script (<https://github.com/yeolab/makebigwigfiles>) which uses bedtools (2.26.0) genomecov to generate normalized density tracks. For analysis of alternative splicing, triplicates of the *Zmat3* knockouts (*E1A;Hras^{G12V};Cas9* MEF lines transduced with lentiviruses expressing one of three unique *Zmat3* sgRNAs) were compared against WT controls (*E1A;Hras^{G12V};Cas9* MEF lines transduced with lentiviruses expressing one of three unique NC sgRNAs) using rMATS (3.2.5) with Gencode (vM15) annotations. Featurecounts (1.5.3) (Liao et al., 2014) was used to count reads mapping to known transcripts using the same vM15 annotations. Differential alternative splicing events were defined by a < 5% change in exon inclusion (PSI or percent-spliced-in > 0.05) and a p value < 0.05.

Comparing ZMAT3 peaks and SMG1-regulated exons

To determine whether ZMAT3 binding is enriched at NMD switch exons, the frequency of ZMAT3 binding peaks was determined for a list of alternative splicing events in SMG1 wild-type and knockout MEFs that were predicted to introduce premature termination codons (PTC) (McIlwain et al., 2010) by identifying the percentage of exons that contain a ZMAT3 peak (sgNC2 sample) anywhere in the region starting at the upstream exon and ending at the downstream exon of the queried exon. This percentage was calculated for PTC-containing exons that are $\geq 5\%$ differentially spliced in the direction that would include the PTC in SMG1 wild-type versus knockout MEFs (SMG1-regulated PTC exon). As one control, the set of PTC-containing exons that are < 1% differentially spliced was similarly compared against ZMAT3 peaks. As another control, sets of 232 internal exons with similar expression levels to the SMG1 regulated exons were randomly selected 10,000 times and compared against ZMAT3 peaks. Significance was calculated by identifying the number of times this random selection identified an equal or greater number of events with overlapping ZMAT3 peaks.

Analysis of DepMap samples

To evaluate genotype-specific dependencies of human cell lines, we categorized all cell lines (including breast, lung, liver, and colon cancer lines) in the Achilles DepMap dataset (CCLE_Depmap_18q3 release) into two categories: *TP53* aberrant or *TP53* wild-type. Cell lines were considered "*TP53* aberrant" if they fulfilled at least one of the following criteria: (1) mRNA expression of *TP53* was at least one standard deviation below the mean of all cell lines tested; AND/OR (2) cell lines were previously annotated as *TP53* mutant ("is Deleterious" criteria could be either TRUE or FALSE) (n = 350 *TP53*-aberrant cell lines). Cell lines were considered "*TP53* wild-type" if they fulfilled both of these criteria: (1) mRNA expression of *TP53* was greater than one standard deviation above the mean of all cell lines tested; AND (2) cell lines were not previously annotated as having a mutation in *TP53* (n = 135 *TP53* wild-type cell lines). We then calculated the mean dependency scores for each gene in the genome for all *TP53* aberrant lines and all *TP53* wild-type lines. We performed two-tailed t tests evaluating the differences in mean dependency scores for each gene and then adjusted the p values

with the Benjamini-Hochberg procedure for multiple comparison testing (generating FDR values). Genes with FDR values < 0.1 were considered significant.

QUANTIFICATION AND STATISTICAL ANALYSIS

A hypergeometric test (i.e., sampling without replacement) was used to calculate significance in the shRNA screen. A Mann-Whitney U test was used to calculate significance in the sgRNA screen. A log-rank test and Cox Proportional Hazard model were used to calculate significance in the survival analyses. The DISCOVER method was used to test for mutual exclusivity. The Benjamini-Hochberg procedure for multiple comparison testing was used to calculate significance in the analysis of DepMap samples. The unpaired two-tailed Student's t test was used for all the other statistical analyses. Error bars represent standard deviation or standard error of the mean (see figure legends). Significance was defined as a p value ≤ 0.05 , unless otherwise stated. Details and significance values can be found in the figure legends.